© 2020. Published by The Company of Biologists Ltd | Development (2020) 147, dev183954. doi:10.1242/dev.183954

RESEARCH ARTICLE

MMP14 is required for delamination of chick neural crest cells independently of its catalytic activity

Cyril Andrieu[1], Audrey Montigny[1], Anne Bibonne[1], Evangeline Despin-Guitard[1], Dominique Alfandari[2] and Eric Théveneau[1,*]

ABSTRACT

Matrix metalloproteinases have a broad spectrum of substrates ranging from extracellular matrix components and adhesion molecules to chemokines and growth factors. Despite being mostly secreted, MMPs have been detected in the cytosol, the mitochondria or the nucleus. Although most of the attention is focused on their role in matrix remodeling, the diversity of their substrates and their complex trafficking open the possibility for non-canonical functions. Yet *in vivo* examples and experimental demonstration of the physiological relevance of such activities are rare. Here, we have used chick neural crest (NC) cells, a highly migratory stem cell population likened to invasive cancer cells, as a model for physiological epithelial-mesenchymal transition (EMT). We demonstrate that MMP14 is required for NC delamination. Interestingly, this role is independent of its cytoplasmic tail and of its catalytic activity. Our *in vivo* data indicate that, in addition to being a late pro-invasive factor, MMP14 is also likely to be an early player, owing to its role in EMT.

KEY WORDS: EMT, MMP14, Delamination, Mitosis, Neural crest, Polarity

INTRODUCTION

Matrix metalloproteinases (MMPs) are widely expressed in cancer and inflammation (Bonnans et al., 2014; Khokha et al., 2013). Most of the attention has been focused on their role in matrix remodeling. However, we now know that MMPs can traffic to various cell compartments, including the nucleus, the mitochondria and the cytosol (Jobin et al., 2017). In addition, numerous non-canonical substrates, unrelated to matrix biology, have been found. It is therefore assumed that MMPs influence a broad range of biological functions, ranging from cell proliferation to differentiation to cell migration (Rodríguez et al., 2010).

MMP14 was the first membrane-bound MMP discovered in 1994 (Sato et al., 1994). MMP14 is expressed in numerous human cancers where it modulates tumor growth and cancer invasion (Turunen et al., 2017). MMP14 is also required in physiological events, such as mammary gland (Feinberg et al., 2016) and bone development (Holmbeck et al., 1999), and skeletal muscle regeneration (Kopinke et al., 2017). In most cases, MMP14 acts via activation of MMP2 and/or degradation of extracellular matrix. However, the range of the substrates of MMP14 extends beyond the matrix. MMP14 can cleave membrane proteins such as CD44 (Suenaga et al., 2005) and ADAM-9 (Chan et al., 2012), or secreted factors such as SDF1 (McQuibban et al., 2001). It can also interact with and process integrins (Gonzalo et al., 2010b). Furthermore, MMP14 can have non-catalytic functions. The cytoplasmic domain contains binding sites for regulators of Rho GTPases (Gonzalo et al., 2010a; Hoshino et al., 2009) and regulators of the transcription factor HIF (Sakamoto and Seiki, 2010; Sakamoto et al., 2014). Finally, MMP14 has been detected inside the nucleus, where it regulates gene expression (Shimizu-Hirota et al., 2012). Most of these non-canonical functions have not been tested *in vivo*. In addition, these observations suggest that MMP14 could be involved in early steps of epithelial-mesenchymal transition (EMT) as Rho GTPases and HIF have been implicated in this process (Barriga et al., 2013; Joseph et al., 2018). During EMT, cells modulate cell-cell and cell-matrix adhesion, remodel their polarity from apico-basal to front-rear and degrade extracellular matrix (Nieto et al., 2016). In human prostate cancer cell lines, MMP14 has been shown to contribute to EMT in a Wnt5a-dependent manner (Cao et al., 2008) and MMP14 can trigger an E- to N-cadherin switch when experimentally overexpressed in esophageal squamous cell carcinoma *in vitro* (Pang et al., 2016). MMP14 was shown to be important for *in vivo* cell migration of *Xenopus* neural crest (NC) cells (Garmon et al., 2018) in the context of an MMP2-positive environment. However, *Xenopus* NC cells migrate as a pseudoepithelial sheet and do not perform the typical basal extrusion from an epithelium observed during carcinoma progression or during NC delamination in amniotes (Mayor and Theveneau, 2013). Thus, a direct involvement of MMP14 in EMT *in vivo* remains to be tested.

Here, we have used chick NC cells as *in vivo* model of EMT. NC cells are a multipotent stem cell population that leaves the neuroepithelium by a series of EMT-driven basal extrusions (Gouignard et al., 2018). We found that MMP14 is expressed by trunk NC cells during EMT. We demonstrate that MMP14 is required for NC delamination. MMP14 does so independently of its catalytic activity and does not affect cadherins or laminin distribution. Instead, MMP14 acts by promoting the occurrence of basal mitoses. Our *in vivo* data place MMP14 as an early player in the EMT cascade.

RESULTS

MMP14 expression prior to and during NC delamination

First, we analyzed the expression of MMP14 by *in situ* hybridization in the trunk of chicken embryos. At stage HH13 (19 somites), MMP14 mRNA is detected in the neural tube, the somites, the notochord and the lateral mesoderm, as seen in whole mount (Fig. 1A) and on transverse sections (Fig. 1B-D). In the NC domain, MMP14 is weakly expressed before EMT (Fig. 1B,C, asterisks). Its expression increases during EMT (Fig. 1D). Owing to the strong expression of MMP14 in somites, it is difficult to identify NC cells expressing MMP14 while they migrate through the

[1]Centre de Biologie du Développement, Centre de Biologie Intégrative, Université de Toulouse, CNRS, UPS, Toulouse, 31062, France. [2]Department of Veterinary and Animal Sciences, University of Massachusetts, Amherst, MA 01003, USA.

*Author for correspondence (eric.theveneau@univ-tlse3.fr)

E.T., 0000-0001-6510-5717

Received 20 August 2019; Accepted 24 February 2020

Development (2020) 147, dev183954. doi:10.1242/dev.183954

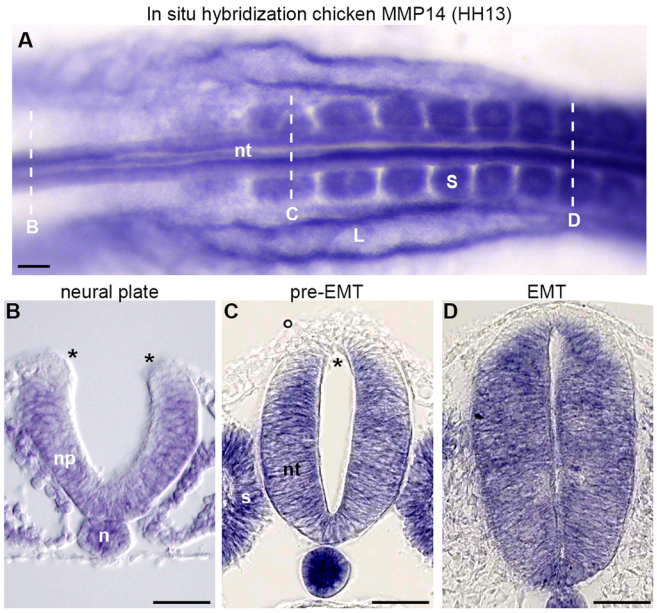

Fig. 1. Expression of MMP14 during EMT of chick NC cells. (A) *In situ* hybridization against chick MMP14. Dorsal view of the caudal part of a stage HH13 chick embryo. Scale bar: 100 µm. (B-D) *In situ* hybridization for chick MMP14. Transverse sections. MMP14 expression is increased in the neural crest during EMT. Scale bars: 50 µm. s, somite; L, lateral mesoderm; np, neural plate; nt, neural tube; n, notochord. Asterisks indicate the pre-migratory NC cells.

paraxial mesoderm. To overcome this issue, we cultured NC cells. In culture, expression of MMP14 is clearly seen in migratory NC cells that have left the neural tube explant (Fig. S1).

MMP14 is required for trunk neural crest delamination independently of its catalytic activity

To assess whether MMP14 is required for NC delamination, we performed loss of function by electroporation with a siRNA against MMP14 or a scrambled version of the siRNA as control (Fig. 2A,B). The siRNA-MMP14 efficiency was tested by western blot (Fig. S2). Twenty-four hours post electroporation (24 hpe), the scrambled control did not affect the size of the NC domain (Fig. 2A,F). However, siRNA-MMP14 led to an accumulation of Snail2-positive NC cells in the dorsal neural tube, shifting the limit of the NC region ventrally (Fig. 2B, bracket; 2F). This effect is not specific to Snail2 and can be observed with other NC markers such as Sox9 (Fig. S3) or AP2 (see Fig. 3 hereafter). We then attempted to rescue MMP14 knockdown by co-expressing GFP-tagged versions of wild-type MMP14 or a point mutant version (MMP14-EA) in which a glutamate essential for the catalytic activity has been replaced by an alanine (Rozanov et al., 2001). Catalytic inactivity of MMP14-EA was confirmed by acceptor photobleaching FRET and by monitoring the cleavage pattern of the FRET reporter by western blot (Fig. S4, see Materials and Methods). Importantly, MMP14-GFP and MMP14-EA-GFP were generated by codon optimization, making them resistant to the siRNA. MMP14 (Fig. 2C) and MMP14-EA (Fig. 2D) were equally capable of preventing accumulation of NC in the dorsal neural tube when co-electroporated with siRNA-MMP14 (Fig. 2F). Such accumulation of NC cells in the dorsal neural tube could be due to an expansion of the NC domain or to a lack of delamination. To distinguish between these two possibilities, we performed a loss-of-function with an alternative method by using an inhibitor of MMP14 (NSC405020) that binds to the hemopexin domain of MMP14 (Remacle et al., 2012). We cultured neural tube explants with NSC405020 or DMSO as control. Exposure to NSC405020 reduced the total number of NC cells outside the neural tube compared with the DMSO (Fig. S5) indicating that blocking MMP14 prevents delamination. Furthermore, we found no effect on proliferation after electroporation with si-RNA-MMP14 or its scrambled control (Fig. S6). Altogether, these results indicate that MMP14 is required for NC delamination from the neural tube and that it acts independently of its catalytic activity. As NC delamination is achieved by EMT in the chicken embryo, these data indicate that MMP14 is involved in EMT.

MMP14 is required for the remodeling of cell polarity during NC delamination

EMT is a complex process that involves a qualitative and quantitative change in cell adhesion, extracellular matrix remodeling, a loss of apicobasal polarity and the acquisition of migratory capabilities (Nieto et al., 2016). Thus, we aimed to identify which of these steps is failing after MMP14 loss-of-function in NC cells. First, we checked the distributions of E and N cadherins, and that of laminin, a component of the basal membrane. E-cadherin expression in the trunk neuroepithelium is lost several hours prior to EMT of NC cells (Dady et al., 2012; Dady and Duband, 2017). N-cadherin is downregulated at transcriptional and post-translational levels at the time of trunk NC delamination (Shoval et al., 2007). Whereas laminin distribution is not complete over the dorsal neural tube during NC EMT (Leonard and Taneyhill, 2019). Thus, a maintenance of any of these three molecules might account for the defect in delamination. However, the loss of MMP14 had no effect on their distributions (Fig. S7). Next, we assessed cell polarity. In the chicken embryo, delamination of trunk NC cells occurs after neural tube closure and, contrary to what is observed at cephalic levels, the epithelial integrity of the dorsal neural tube is maintained throughout the whole delamination process. That is due to the fact that trunk NC cells undergo EMT one cell at a time. Thus, any given delaminating cell is surrounded by non-delaminating cells that retain their normal adherence junctions and polarity markers. Therefore, apical markers such as aPKC or ZO1 are always present in the dorsal neural tube. In addition, such apical markers are no longer detectable in cells undergoing EMT and accumulate relatively late during epithelialization (Fig. S8). Thus, they are not informative when it comes to analyzing an experimental condition in which cells are prevented from leaving the neural tube, as observed with siRNA-MMP14 (Fig. 3A,B). By contrast, we found that pericentriolar material 1 (PCM1) subcellular localization clearly changes when cells toggle between epithelial and mesenchymal phenotypes, e.g. during secondary neurulation or mesoderm development (somite epithelialization, EMT of the sclerotome) (Fig. S8). More precisely, PCM1 is localized apically early on during epithelialization and remains detectable in cells that have undergone EMT. This is likely due to the fact that PCM1 is not a strict apical marker but is a protein found throughout the cytoplasm that preferentially associates with centrioles and microtubules, and that modulates the centrosomal actin network (Farina et al., 2016). Therefore, we assessed PCM1 distribution in the neural tube at the time of NC delamination. We found PCM1 to be apically biased in neuroepithelial cells. However, in NC cells undergoing EMT, PCM1 is relocated randomly (Fig. 3C-D′, arrowheads) and this change is not affected by the scrambled control (Fig. 3C). On the contrary, siRNA-MMP14 prevented the relocalization of PCM1 in AP2-positive NC cells that were retained in the dorsal neural tube (Fig. 3D,D′, arrows).

Development (2020) 147, dev183954. doi:10.1242/dev.183954

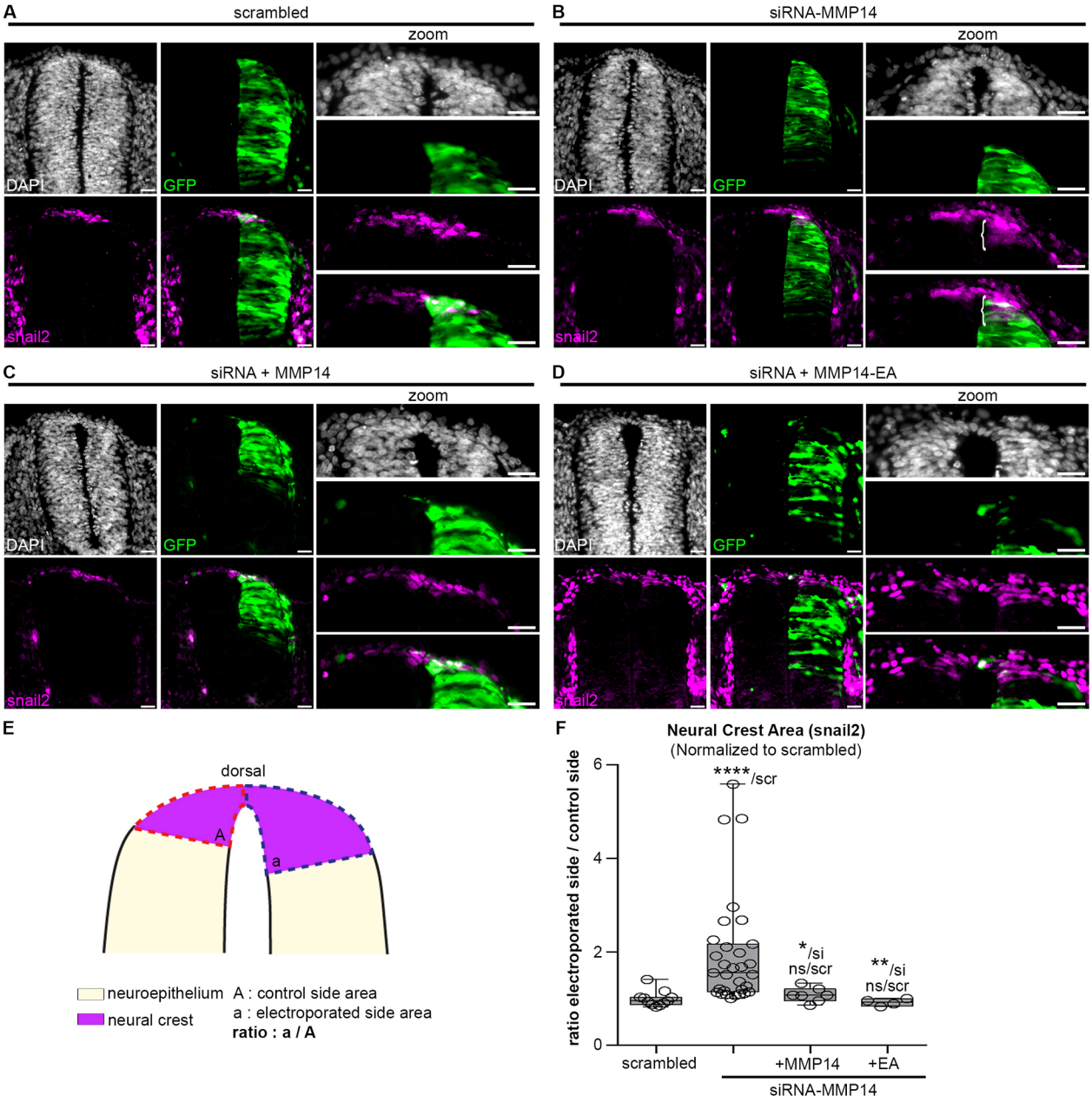

Fig. 2. MMP14 is required for NC delamination independently of its catalytic activity. (A-D) Immunostaining for snail 2 (magenta) after electroporation of scrambled control (A), siRNA-MMP14 (B) and co-electroporation of siRNA-MMP14 with wild-type MMP14 (C) or the non-catalytic point mutant MMP14-EA (D). Nuclei are counterstained with DAPI (grey); the electroporated side is visualized using GFP (green). Brackets indicate neural crest accumulation (B). Scale bars: 20 µm. (E) The method for measuring the area of the neural crest domain. The neural crest area on the electroporated side was divided by the neural crest area in the control side. (F) Plot of neural crest area (snail 2) with scrambled ($n_{embryos}$=11, $n_{sections}$=132 from three independent experiments), siRNA-MMP14 alone ($n_{embryos}$=31, $n_{sections}$=445 from eight independent experiments), siRNA-MMP14 with wild-type MMP14 ($n_{embryos}$=7, $n_{sections}$=134 from two independent experiments) and siRNA-MMP14 with MMP14-EA ($n_{embryos}$=4, $n_{sections}$=90 from one experiment). ANOVA with a Kruskal–Wallis Test and Dunn's multiple comparisons: ****P<0.0001 (scrambled versus siRNA), *P=0.0441 (siRNA versus siRNA+MMP14), **P=0.0030 (siRNA versus siRNA+EA) and P>0.9999 (not significant; scrambled versus siRNA+MMP14 or siRNA+EA).

In the neuroepithelium, mitoses are strictly apical and one can force some cells to divide basally by interfering with apicobasal polarity (Afonso and Henrique, 2006). During NC EMT, basal mitoses have been observed and can be either explained by apical detachment or the loss of apicobasal polarity (Ahlstrom and Erickson, 2009). Thus, we decided to analyze the distribution of mitoses after MMP14 loss of function. We labeled mitotic nuclei using phospho-histone H3 (Fig. 4, pH3). The scrambled control had no effect on the position of mitoses (Fig. 4A) and we found the same percentage of non-apical mitoses on non-electroporated and electroporated sides (Fig. 4C-E). However, the siRNA-MMP14 (Fig. 4B) decreased the proportion of basal mitoses in the NC domain from 37% to 13% (Fig. 4C-E). Despite having a strong effect, MMP14 knockdown does not completely abolish the occurrence of basal mitoses. As we found no effect of siRNA-MMP14 on the normal reduction of N-cadherin occurring in the NC domain (Fig. S7), the remaining 13% of basal mitoses likely correspond to NC cells that had already detached apically.

Development (2020) 147, dev183954. doi:10.1242/dev.183954

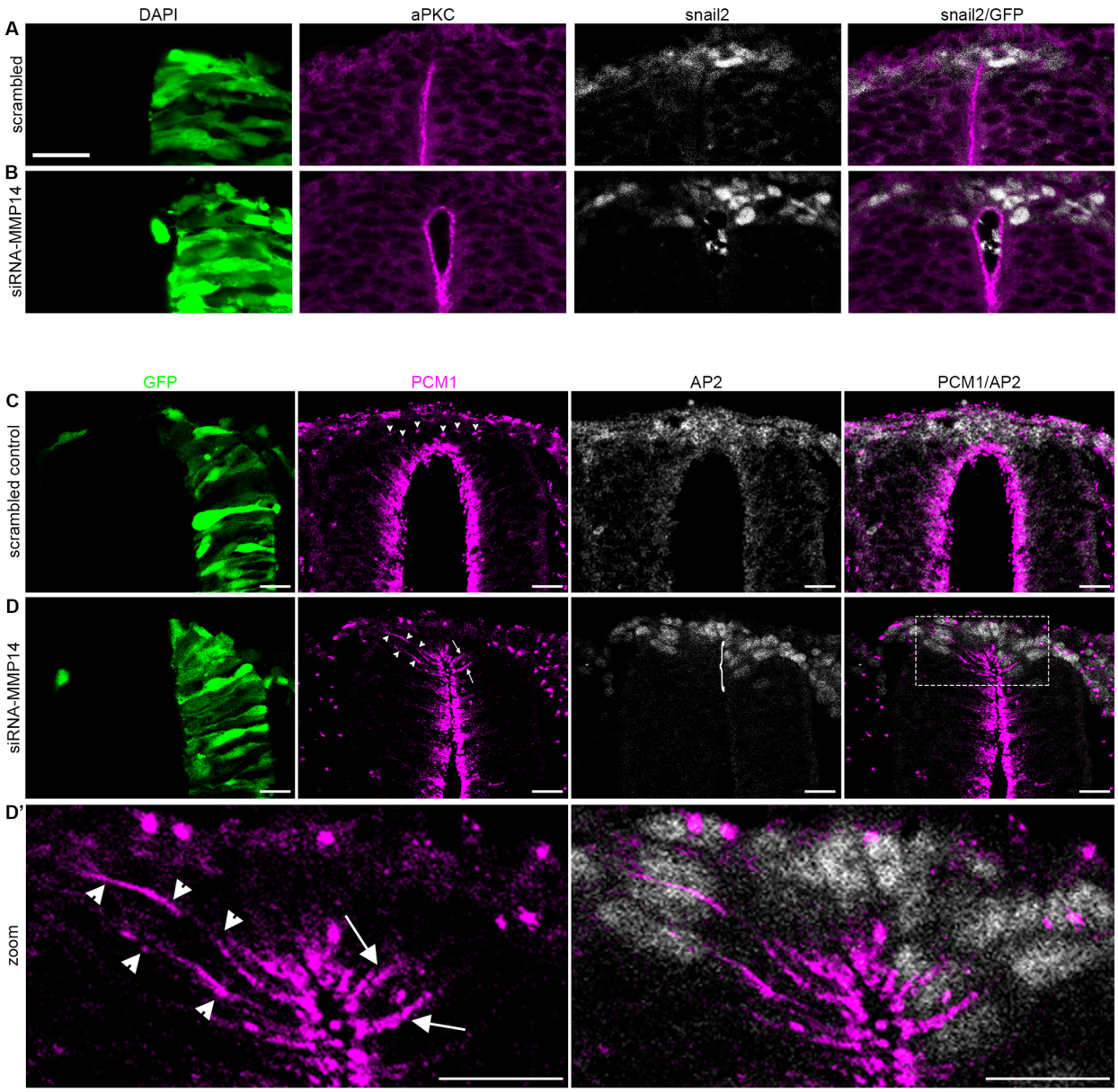

Fig. 3. MMP14 inhibition prevents the apicobasal redistribution of PCM1 during NC EMT. (A,B) immunostaining against aPKC (magenta) and snail 2 (gray) in embryos electroporated with scrambled control (A, $n_{embryos}$=3) and with siRNA-MMP14 (B, $n_{embryos}$=5) from one experiment. (C-D′) Immunostaining against PCM1 (magenta) and AP2 (gray) in embryos electroporated with scrambled control (C, $n_{embryos}$=6) and with siRNA-MMP14 (D,D′, $n_{embryos}$=5) from two independent experiments. (D′) More detail of the neural crest domain. Electroporated side is visualized using GFP (green). Bracket in D indicates the accumulation of neural crest cells. Arrowheads in C indicate the normal basolateral distribution of PCM1 on both non-electroporated and electroporated sides of embryos electroporated with the scrambled control. Arrowheads in D,D′ indicate the normal basolateral distribution of PCM1 on the control side of siRNA-MMP14 embryos. Arrows in D,D′ indicate the apical position of PCM1 on the electroporated side of siRNA-MMP14 embryos. Scale bars: 20 µm.

It has previously been shown that some NC cells delaminate by forming a protrusion, grabbing onto the extracellular matrix and extracting their cell body, sometimes leaving the apical tail within the neuroepithelium (Ahlstrom and Erickson, 2009). Therefore, impairing migratory capabilities could contribute to a delamination defect and NC accumulation in the dorsal neural tube. Thus, we wondered whether the loss of MMP14 might also impair the migratory capabilities of NC cells. To this end, we analyzed the distribution of electroporated cells in the anterior trunk region of embryos expressing the scrambled control or siRNA-MMP14 at 24 hpe. To detect the full extent of NC migration, we counterstained for HNK1 (see Materials and Methods). In control conditions, GFP^+ cells migrate as well as non-electroporated HNK1-positive migratory NC cells, whereas siRNA-MMP14 cells were mostly detected close to the dorsal region of the neural tube (Fig. S9). On the one hand, this migration defect could be due the aforementioned defect of delamination, causing cells to depart with a delay. On the other hand, it could indicate a defect of cell motility per se. To address this, we cultured electroporated neural tube explants on fibronectin (Fig. S10). The siRNA-MMP14 led to fewer GFP-positive NC cells outside the neural tube compared with the scrambled control, confirming that MMP14 knocked-down cells have problems delaminating. However, the mean area explored by the electroporated cells was similar in both conditions. This indicates that, once they have left the neural tube, NC cells electroporated by the scrambled control and the siRNA-MMP14 seem to migrate as efficiently.

Development (2020) 147, dev183954. doi:10.1242/dev.183954

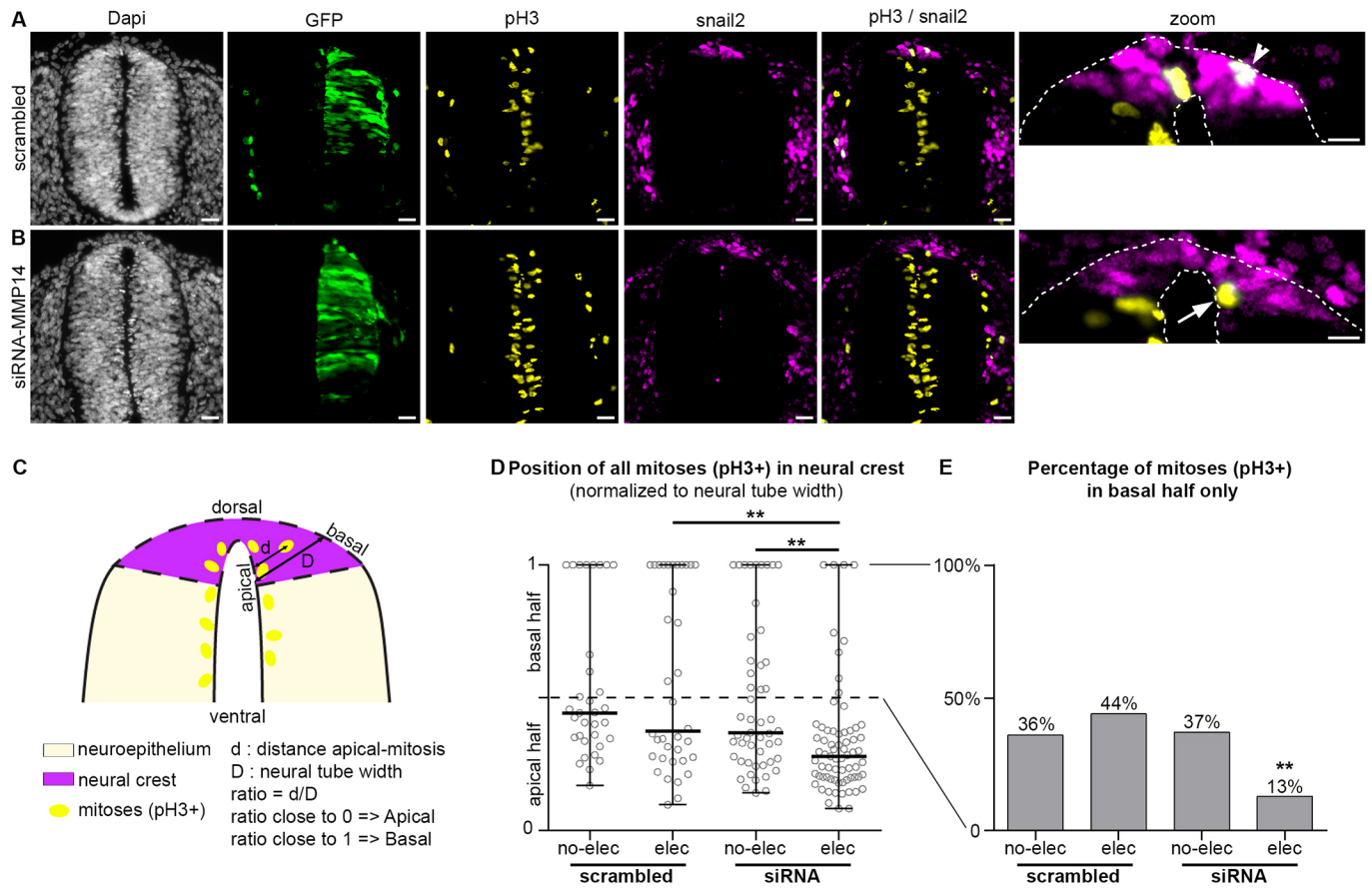

Fig. 4. MMP14 is required for the occurrence of basal mitoses during NC delamination. (A,B) Immunostaining for phospho-histone 3 (pH3) (yellow) and snail 2 (magenta) in electroporated embryos with scrambled control (A) and siRNA-MMP14 (B). GFP is shown in green, nuclei are counterstained with DAPI (gray). Arrowhead in A indicates an example of basal mitosis in the electroporated side. Arrow in B indicates an example of apical mitosis in the electroporated side. Scale bars: 20 µm. (C) Diagram depicting the method of measuring the positions of mitoses along the apical-basal axis. The distance between the mitoses and the apical part of neural tube (d) was divided by the neural tube width (D). A ratio of 0 means that the mitoses were close to the apical region. A ratio of 1 means that the mitoses were close to the basal region. (D) Plot of the position of the mitoses along the apico-basal axis in the neural crest in embryos electroporated with the scrambled control ($n_{embryos}$=3, $n_{mitoses\ non\text{-}elec\ side}$=33, $n_{mitoses\ elec\ side}$=36 from one experiment) or siRNA-MMP14 ($n_{embryos}$=8, $n_{mitoses\ non\text{-}elec\ side}$=51, $n_{mitoses\ elec\ side}$=69, from three independent experiments). Dashed line indicates the border between the apical half and basal half. ANOVA followed by Dunn's multiple comparisons **P=0.0014 (electroporated scrambled versus electroporated siRNA), **P=0.0027 (non-electroporated siRNA versus electroporated siRNA). In the scatter dot plot, the lines indicate the median and the error bars show the extent of the whole dataset. (E) Percentage of basal mitoses in neural crest domain. Basal mitoses were defined as mitoses located within the basal half of the neural crest domain (corresponding to values between 0.5 and 1 on the graph in D). Statistics were performed according to Taillard et al. (2008), **T>6.635 (non-electroporated siRNA versus electroporated siRNA) the null hypothesis is rejected with 99% confidence. No-elec, non-electroporated side; elec, electroporated side.

Altogether, these data indicate that: (1) MMP14 has no effect on E or N cadherins or on laminin distribution in the dorsal neural tube; (2) MMP14 does not seem to affect the intrinsic motility of NC cells; and (3) MMP14 is required for basal positioning of mitoses during NC EMT.

Overexpression of MMP14 is sufficient to promote basal mitosis in the neuroepithelium

We next wondered whether the endogenous expression of MMP14 in the neuroepithelium is required for the normal apical positioning of mitoses and whether upregulating MMP14 might be sufficient to trigger basal mitosis. We first analyzed the effect of the scrambled control and the siRNA-MMP14 in the neuroepithelium. They had no effect on the distribution of mitoses (Fig. 5A,B), indicating that neuroepithelial cells do not require MMP14 to maintain normal apicobasal polarity and normal interkinetic nuclear movements. Next, to assess whether MMP14 is sufficient to promote non-apical mitosis, we overexpressed different GFP-tagged forms of MMP14 in the neuroepithelium: wild-type MMP14, the inactive point mutant (MMP14-EA), a delta-catalytic form (MMP14-ΔCAT) or a delta-cytoplasmic form (MMP14-ΔCyto) (Fig. 5C). All forms of MMP14 distributed homogenously along the apicobasal axis (Fig. 5D) and were able to promote non-apical mitosis (Fig. 5D, arrows; 5E,F). As neuroepithelial cells robustly divide with their nuclei in an apical position, we determined that non-apical mitoses occurred more than two nuclei diameters away from the apical domain. In non-electroporated halves of the neural tubes, used as internal controls, only 1.7% of non-apical mitoses were observed (Fig. 5F), whereas overexpression of MMP14 or MMP14-EA led to a threefold increase in the number of non-apical mitoses to 5% and 5.2%, respectively (Fig. 5F). MMP14-ΔCAT had a weaker effect, producing 3.3% of non-apical mitoses, whereas MMP14-ΔCyto had a stronger effect, producing 10.2% of non-apical mitoses (Fig. 5F). Altogether, these results indicate that increasing MMP14 expression is sufficient to promote basal mitoses independently of the catalytic activity or the cytoplasmic tail. Importantly, overexpression of

Development (2020) 147, dev183954. doi:10.1242/dev.183954

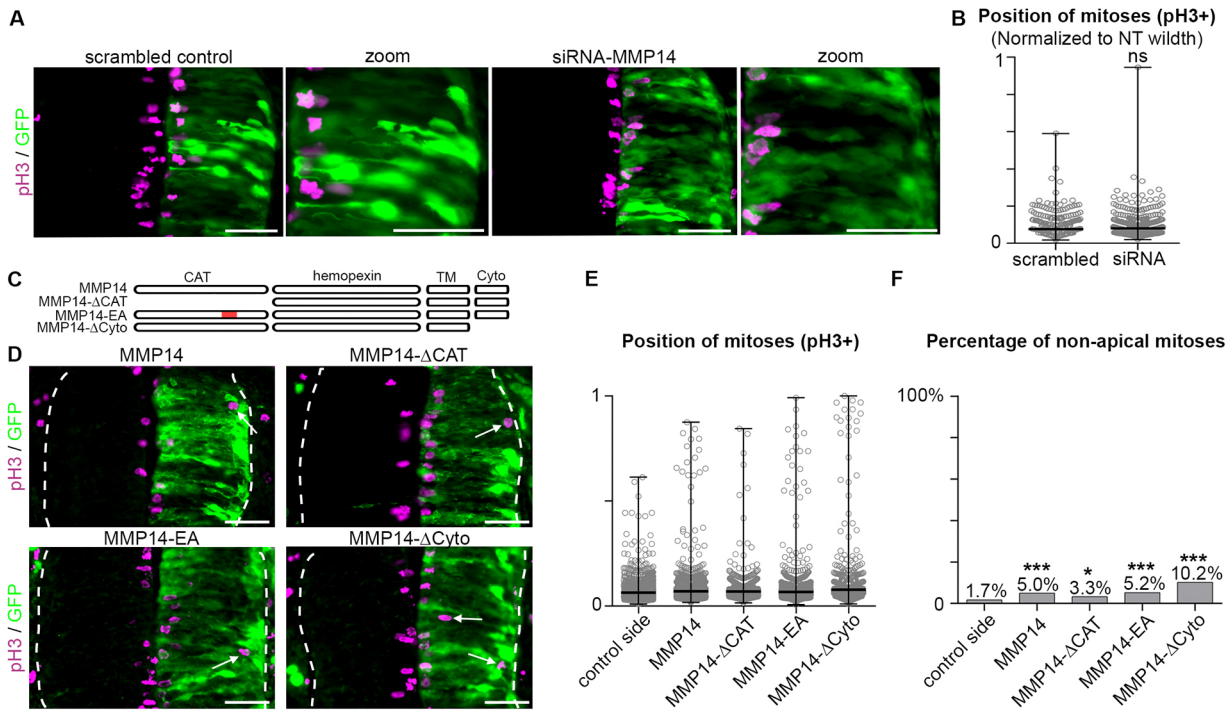

Fig. 5. Homogenous distribution of MMP14 is sufficient to promote basal mitoses independently of its catalytic activity. (A) Immunostaining against phospho-histone H3 (pH3, magenta) after electroporation with the scrambled control or siRNA-MMP14. (B) Positions of mitoses in the intermediate neural tube region with the scrambled control ($n_{embryos}$=6, $n_{mitoses}$=339; from two independent experiments) or siRNA-MMP14 ($n_{embryos}$=11, $n_{mitoses}$=362; from four independent experiments). Unpaired Mann–Whitney test, P=0.7780. (C) Diagram depicting the different forms of MMP14. (D) Immunostaining against pH3 (magenta) after overexpression of MMP14, MMP14-ΔCAT, MMP14-EA and MMP14-ΔCyto. Arrows indicate non-apical mitoses. (E) Positions of all mitoses for each condition depicted in D. Control side ($n_{embryos}$=26, $n_{mitoses}$=1908), MMP14 ($n_{embryos}$=7, $n_{mitoses}$=716), MMP14-ΔCAT ($n_{embryos}$=7, $n_{mitoses}$=406) and MMP14-EA ($n_{embryos}$=9, $n_{mitoses}$=707) from three independent experiments, and MMP14-ΔCyto ($n_{embryos}$=3, $n_{mitoses}$=431) from one experiment. (F) Percentages of non-apical mitoses for each condition depicted in D. Non-apical mitoses were determined as mitoses occurring more than two nuclei diameters away from the apical domain. Statistics were performed according to Taillard et al. (2008), Thresholds for T were such that, at *T>3.841, the null hypothesis is rejected with a 95% confidence, at **T>6.635, the null hypothesis is rejected with 99% confidence and at ***T>10.83, the null hypothesis is rejected with 99.9% confidence. In B,E, the lines indicate the median and the error bars show the extent of the whole dataset. Electroporated side is indicated by GFP (A,D, green). Scale bars: 35 µm.

MMP14 in the neural tube is not sufficient to promote ectopic EMT, as we observed neither a loss of N-cadherin in electroporated cells nor a local degradation of laminin next to them (Fig. S11). These data demonstrate that the non-apical mitoses induced by MMP14 are not caused by a local induction of EMT and confirm a specific role for MMP14 in nuclear positioning that is independent of its catalytic function.

We next wondered whether destabilizing apicobasal polarity in the NC domain would be sufficient to compensate for the lack of MMP14. To investigate this, we made use of Par3 overexpression, previously described as sufficient to cause non-apical mitoses in the chick neuroepithelium without causing ectopic delamination of neuroepithelial cells (Afonso and Henrique, 2006). Importantly, the accumulation of NC in the dorsal neural tube induced by siRNA-MMP14 can be rescued by Par3 overexpression (Fig. 6A,B).

Par3 has been implicated in the regulation of cell migration (e.g. Moore et al., 2013; Nishimura and Kaibuchi, 2007; Pegtel et al., 2007). Thus, one could suggest that overexpressing Par3 might compensate for the lack of MMP14 by promoting delamination independently of its effect on cell polarity. To circumvent this, we

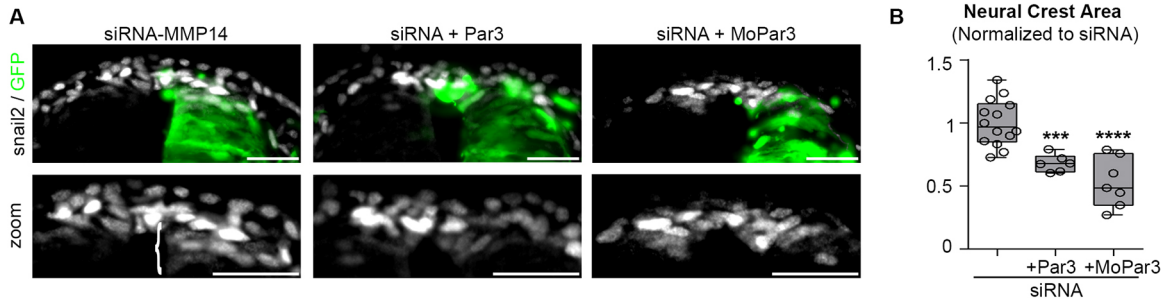

Fig. 6. Destabilizing apicobasal polarity is sufficient to rescue siRNA-MMP14. (A) Immunostaining for snail 2 (gray) after electroporation of siRNA-MMP14 or co-electroporation with siRNA-MMP14 and Par3. Bracket indicates accumulation of neural crest cells. (B) Plot of neural crest area (snail 2) with siRNA-MMP14 ($n_{embryos}$=14, $n_{sections}$=361), siRNA-MMP14 with Par3 ($n_{embryos}$=6, $n_{sections}$=166) and siRNA-MMP14 with Par3MO ($n_{embryos}$=7, $n_{sections}$=38) from two independent experiments. ANOVA and uncorrected Fisher's LSD; ***P=0.0007, ****P<0.0001. Scale bars: 25 µm. Par3MO efficiency/specificity could not be checked (see main text and Materials and Methods for details).

Development (2020) 147, dev183954. doi:10.1242/dev.183954

attempted to rescue MMP14 knockdown by performing Par3 loss of function experiments. We designed a translation-blocking morpholino against chicken Par3 (Par3MO). Electroporation of Par3MO in the neural tube has only mild effects, leading to occasional ectopic mitoses, basal accumulation of nuclei and some basal rosette-like organization of nuclei, all indicative of mild apico-basal polarity defects (Fig. S12). Importantly, the overall structure of the neural tube is intact and no ectopic delaminate or EMT-like phenotype is observed. Co-electroporation of siRNA-MMP14 and Par3MO was sufficient to prevent the accumulation of snail2-positive NC cells in the dorsal neural tube (Fig. 6A,B). However, these data should be taken with caution. It is important to note that we were unable to check for the Par3MO efficiency by immunostaining or western blots as the two anti-Par3 antibodies we have tested did not produce specific signals (see Materials and Methods). In addition, assessment for specificity by a rescue strategy of the Par3MO is not possible because expression of Par3 alone also leads to apico-basal defects (Afonso and Henrique, 2006). The mild effects observed after Par3MO electroporation are in line with Par3 loss-of-function data published elsewhere (Chuykin et al., 2018), suggesting that the knockdown is efficient; however, readers may decide to ignore these data due to the lack of formal validation of Par3MO.

DISCUSSION

The first MMP was identified as a collagenolytic enzyme in tadpoles (Gross and Lapiere, 1962). Since then, more than 20 MMPs have been discovered in vertebrates. The vast majority of publications on MMPs has focused on their roles in extracellular matrix remodeling, most of these works being conducted *in vitro* either from a purely biochemical perspective or in cell culture. It is unfortunate, because MMPs have a much broader range of capabilities. MMPs have a secretion peptide in their N terminus but are not restricted to the extracellular space. MMPs have been found in the cytoplasm, the mitochondria and the nucleus, indicating that we still know very little about how their trafficking is controlled. In addition, several non-proteolytic activities, including signaling or transcription, have been found. (For reviews on the non-canonical roles and subcellular localizations of MMPs, see Iyer et al., 2012; Jobin et al., 2017; Mannello and Medda, 2012.) Here, our data provide one of the very few *in vivo* examples of a physiologically relevant non-catalytic MMP activity by showing that MMP14 is essential for NC delamination.

MMP14 expression is often associated with poor prognosis in cancers such as colorectal, breast and stomach (Cui et al., 2019; Dong et al., 2015; Yao et al., 2013). Here, we found MMP14 mRNA in numerous epithelial structures, such as the neuroepithelium, the notochord and the epithelial somites. These data indicate that, contrary to other MMPs, such as MMP2 (Duong and Erickson, 2004), MMP14 gene expression is not systematically linked to EMT or to cell migration during early development.

Our *in vivo* and *in vitro* experiments show that knocking down MMP14 reduces the number of delaminating NC cells but does not seem to affect their intrinsic motility. In addition, adjacent cells that were not electroporated with siRNA-MMP14 were not affected. These data indicate that MMP14 is specifically required for delamination and acts cell autonomously. Our *in vitro* results do not completely rule out the possibility that MMP14 may play a role in NC migration *in vivo* as cells are known to adopt different migratory behaviors in 3D and 2D environments (Caswell and Zech, 2018). In addition, proteolytic enzymes are extremely versatile, and demonstrating a non-proteolytic role in one phenomenon does preclude a catalytic function of the same enzyme once cells are in a different context (e.g. located within the extracellular matrix after delamination). Interestingly, trunk NC cells in chick migrate through an environment rich in stromal cell-derived factor 1 (Sdf1/CXCL12) (Saito et al., 2012) and fibronectin (Perris and Perissinotto, 2000), and NC cells need Sdf1 to reach the anlagen of the sympathetic ganglia (Kasemeier-Kulesa et al., 2010). Interestingly, Sdf1 displays a high affinity for fibronectin (Pelletier et al., 2000), suggesting that most of the secreted Sdf1 might be trapped in fibronectin-rich matrices *in vivo*. Both fibronectin and Sdf1 are substrates of MMP14 (Barbolina and Stack, 2008; Shi and Sottile, 2011). More specifically, MMP14 can render Sdf1 inactive by removing the first four amino acids in its N terminus (McQuibban et al., 2001). Therefore, one possibility is that, despite being involved in NC delamination in a non-proteolytic manner, MMP14 might later contribute to the normal dorsoventral migration of trunk NC cells *in vivo* by first promoting the release of Sdf1 from fibronectin and subsequently inactivating it by removing its N terminus. The shorter migration observed in siRNA-MMP14 transfected cells would be the result of a delayed delamination due to polarity defects and additional migration defects. Such migration defects would not be detectable in our 2D *in vitro* assays, as they are performed on ready-to-use fibronectin and in the absence of Sdf1. This possibility, which is well beyond the scope of our study, remains to be explored.

Delamination of trunk NC cells is known to be bound to the G1/S transition of the cell cycle (Burstyn-Cohen and Kalcheim, 2002). Owing to interkinetic movements, nuclei are located basally when cells are in S phase and apically in mitosis (Spear and Erickson, 2012). It has been proposed that blocking cells from entering in S phase hinders NC delamination by retaining nuclei in an apical position (Burstyn-Cohen and Kalcheim, 2002). However, the fact that NC cells lose their apicobasal polarity and display a high rate of basal mitosis indicates that basal positioning of NC nuclei is no longer tightly linked to interkinetic movements during NC EMT. Therefore, part of the previously described effect of blocking the G1/S transition may be due to blocking proliferation (Burstyn-Cohen and Kalcheim, 2002). Our data show that the percentage of NC cells undergoing basal mitosis depends on the presence of MMP14. Importantly, this happens in absence of effects on the overall proportion of $pH3^{+}$ cells ruling out the possibility that MMP14 acts on proliferation itself.

How can MMP14 modulate apicobasal polarity? One possibility is via its cytoplasmic tail. The cytoplasmic tail of mammalian MMP14 is known to harbor binding sites for regulators of Rac1 and RhoA pathways (Gonzalo et al., 2010a; Hoshino et al., 2009), which could link MMP14 to the regulation of apicobasal polarity. However, several of these sites are absent in the sequence of chicken MMP14 (Yang et al., 2008). In addition, the truncated form MMP14-ΔCyto was sufficient to promote non-apical mitosis in the neuroepithelium, indicating that MMP14 can act on polarity without direct intracellular signaling events. In particular, the effect of MMP14-ΔCyto strongly suggests that a direct interaction between MMP14 and the Par complex is unlikely. MMP14-ΔCyto provoked twice as many non-apical mitoses as wild-type MMP14. The cytoplasmic tail of MMP14 is required for normal turnover and endocytosis of MMP14 (Jiang et al., 2001; Uekita et al., 2001). Thus, the MMP14-ΔCyto form is likely to accumulate in the membrane more than the other forms, which may account for its stronger effect. Interestingly, as MMP14 is capable of auto-catalysis, cells that have a high level of MMP14 at the cell surface do not exhibit a significant MMP14-dependent activity. High

Development (2020) 147, dev183954. doi:10.1242/dev.183954

MMP14 activity is instead linked to a rapid turnover and vesicular localization.

This, for example, has been shown in human endothelial cells in which membrane colocalization of MMP14 with β1-integrin is linked to low proteolytic activity and an epithelial phenotype, whereas vesicular MMP14 colocalizing with β3-integrin is associated with high catalytic activity and a migratory phenotype (Gálvez et al., 2002). In this context, a higher membrane accumulation of the ΔCyto form would lead to low catalytic activity due to auto-catalysis. Therefore, the fact that this truncated form is a potent inducer of non-apical mitoses further reinforces the notion that MMP14 acts independently of its catalytic activity, which is demonstrated by the ability of the MMP14 point mutant to rescue MMP14 knockdown and to promote non-apical mitoses as efficiently as wild-type MMP14. Interestingly, the ΔCAT form was less potent at inducing non-apical mitoses than all the other forms of MMP14, indicating that, even if it acts independently of its proteolytic activity, MMP14 requires its complete extracellular domain. This suggests that MMP14 most likely needs to interact with extracellular factors to impact cell polarity and nuclear positioning.

In conclusion, our data show that MMP14 mRNA expression does not correlate systematically with EMT and cell migration, contrary to what has been proposed for other MMPs such as MMP2 (Duong and Erickson, 2004). Importantly, our *in vivo* data demonstrate a direct role of MMP14 in the basal positioning of nuclei during EMT, which is independent of its catalytic activity and independent of cell-cell or cell-matrix adhesion remodeling. MMP14 is often expressed in human cancers (Castro-Castro et al., 2016) and, being an MMP, it is assumed to be a downstream effector of the EMT pathway involved in the matrix degradation that favors tissue invasion. However, our data indicate that MMP14 is specifically required for EMT and that, via this effect, MMP14 plays a crucial role in basal extrusion and thus may act from the onset of invasion. Therefore, it may be worth assessing the putative roles of MMP14 in the early, rather than the late, steps of cancer progression.

MATERIALS AND METHODS

Chicken eggs

Fertilized chicken eggs were purchased from S.C.A.L. (Société commerciale avicole du Languedoc) and incubated at 38°C until the desired stage (Hamburger and Hamilton, 1992).

Electroporation

Embryos at stage HH12 were windowed. Using a glass capillary, a solution of 6% sucrose, 0.05% Fast Green and the expression vector was injected into the lumen of the posterior neural tube. A drop of PBS with antibiotic is added before closing the egg and incubating it overnight. Scrambled and siRNA vectors were electroporated at 1.5 µg/µl. All forms of MMP14 were electroporated at 1-1.5 µg/µl. Par3 vector (Afonso and Henrique, 2006) was electroporated at 0.6 µg/µl. The Par3MO was electroporated at 500 µM.

Antibody against MMP14

Full-length chick MMP14-Flag was expressed in human HEK293T cells using Extreme gene HP (Sigma, 6366244001) and purified using anti-Flag-agarose beads (Sigma, M8823). Balbc mice (Jackson Laboratories) were immunized with 100 µl of purified MMP14-Flag with beads using complete and incomplete Freund's adjuvant. Tail bleeds were collected after two boosts and were tested against Hek293T cells transfected with Chick MMP14 and RFP-Flag (negative control).

Whole-mount immunostaining

After fixation in 4% paraformaldehyde, embryos were washed in 1×PBS/0.1% Tween and incubated for 30-60 min in 1×PBS/1% Triton. Embryos were incubated for 2-3 h in 1×PBS/2% newborn calf serum. Embryos were incubated with primary antibody in 1×PBS/2% newborn calf serum/0.1% Triton for 24-48 h at 4°C. Embryos were washed in 1×PBS/0.1% Tween and incubated with secondary antibody in 1×PBS overnight at 4°C. Embryos were washed in 1×PBS/0.1% Tween before observation or embedding for histology.

Histology

After fixation in 4% paraformaldehyde or immunostaining, embryos were washed in phosphate buffer (PB) and incubated in PB/15% sucrose overnight at 4°C. Embryos were transferred in PB/15% sucrose/7.5% gelatin (PBSG) for 2 h at 42°C. Small weighting boats were used as molds. A thin layer of PBSG was deposited at the bottom and left to set. Embryos were transferred onto the layer using a plastic 2.5 ml pipette. Each embryo was placed in a drop of PBSG. When drops were set, the weighting boat was filled with PBSG and left to set on the bench. The dish was incubated at 4°C for 1 h to harden the gelatin. Individual blocks were cut under a dissecting microscope to position the embryo in the desired orientation for sectioning. Blocks were frozen in isopentane (Sigma, 615838) at −70°C and stored at −70°C until sectioning.

Cryosections and immunostaining

Cryosections were performed using a cryostat Leica CM1950, as previously described (Théveneau et al., 2007). Sections of 14 µm were incubated in 1×PBS for 30 min at 42°C to remove gelatin, treated with PBS1X/1% triton/2% newborn calf serum for 1 h for permeabilization and blocking. Primary antibodies were diluted in 1×PBS/0.1% Triton/2% newborn calf serum. Sections were incubated with primary antibodies overnight at 4°C under a coverslip. Secondary antibodies were diluted in 1×PBS and applied on sections for 2 h at room temperature. All washes were carried out in 1×PBS. Antibodies used were custom-made polyclonal mouse anti-chick MMP14 (1/500), mouse anti-N-cadherin (DSHB, 6B3, 1/250), mouse anti-E-cadherin (BD Transduction Laboratories, 61081, 1/250), rabbit anti-snail2 (Cell Signaling, C19G7, 1/250), rabbit anti-Sox9 (Millipore, AB5535, 1/100), rabbit anti-sox10 (GeneTex GTX128374, 1/200), mouse anti-TFAP2α (DSHB, 3B5, 1/400), rabbit anti-PCM1 (Dammermann and Merdes, 2002; 1/400), mouse anti-phospho-histone 3 (Ser10) (Cell Signaling, MA312B, 1/1000), mouse anti-laminin (DSHB, 3H11, 1/100), mouse anti-HNK1 (DSHB, 1C10, 1/50), mouse anti-aPKC (Santa Cruz, sc17781, 1/100), mouse anti-ZO1 (ThermoFisher, 33-9100, 1/200) and mouse anti-β-catenin (Sigma, C2206, 1/200). We attempted to use rabbit anti-mouse Par3 and mouse anti-human Par3 (Millipore, 07-330 and 8E8) but none of them produced staining that was specific for chicken Par3. Ab 07-330 has previously been used in chicken but given that it is a rabbit polyclonal antibody that targets mouse Par3 the batch we purchased might not be crossreacting efficiently with the chicken protein. All secondary antibodies were coupled with Alexa 488, 555/594 or 633/647 (Invitrogen). The anti-HNK-1 antibody detects a carbohydrate post-translational modification found on numerous cell-surface molecules, including N-CAM. This epitope is strongly detected in chicken NC cells and is commonly used as a marker (Giovannone et al., 2015).

siRNA and morpholinos

siRNA-MMP14 and scrambled control were cloned in a pGFP RNAi vector. The target sequence, the primers used and the final siRNA sequence are as follows for each construct: siRNA-MMP14 targets 5′-GGAAGTGTCGACCCGGAAA-3′, forward primer is 5′-gagaggtgctgctgagcgAGAAGTGTCGACCCGGAAATAGTGAAGCCACAGATGTA-3′, reverse primer is 5′-attcaccaccactaggcaGGAAGTGTCGACCCGGAAATACATCTGTGGCTTCACT-3′ and final sequence siRNA-MMP14 primer is 5′-ggcggggctagctggagaagatgccttccggagaggtgctgctgagcgAGAAGTGTCGACCCGGAAATAGTGAAGCCACAGATGTATTTCCGGGTCGACACTTCCtgcctagtggtggtgaatagcggggttagaagctttcttcccctcttcttaagccaccc-3′; the scrambled control targets 5′-ACGGACTAGCTAAGGACGG-3′, forward primer is 5′-gagaggtgctgctgagcgCCGGACTAGCTAAGGACGGtagtgaagccacagatgta-3′, reverse primer is 5′-attcaccaccactaggcaACGGACTAGCTAAGGACGGtacatctgtggcttcact-3′ and final sequence scrambled control primer is 5′-ggcggggctagctggagaagatgccttccggagaggtgctgctgagcgCCGGACTAGC-TAAGGACGGTAGTGAAGCCACAGATGTACCGTCCTTAGCTAGTCCGTtgcctagtggtggtgAatagcggggttagaagctttcttcccctcttcttaagccaccc-3′.

Development (2020) 147, dev183954. doi:10.1242/dev.183954

The Par3 morpholino was designed to target the ATG codon and was produced by Genetools. The sequence of the Par3 morpholino is 5′-gaagcacacggtgactttcatcctg-3′.

In situ hybridization

Whole-mount *in situ* hybridization was performed as previously described (Théveneau et al., 2007). The probe against chick-MMP14 targets the following sequence:

5′-GACGGCGGCTTCGATACCATCGCGGTGCTCAGGGGGGAGAT-GTTCGTGTTCAAGGAGCGGTGGCTGTGGCGGCTGCGGGAGCG-CCGGGTGCTGCCCGGTTACCCCCTCCCTATGGGGCAGCTGTGG-CCCGGACTGCCCCACAGCATCGACGCCGCCTATGAGAGGAAG-GACGGCAAGTTCGTCTTCTTCAAAGGCGGGCGGCAGTGGGTG-TTCTCGGAGGCGGCGCTGCAGCCGGGCTTCCCGCGCGCTCTG-CCGGACGTGGGCCGGGGGCTGCCGGAGCGCATCGACGCCGCG-CTGCTGTGGCTGCCCAGCGGGGCCACGTACCTCTTCCGGGGC-GACAAGTACTACCGGTTCAATGAGGAGACGGAGTCGGTGGAC-CCCGATTACCCCAAAAGCATTTCCGTGTGGGGCGGCGTCCCCG-AATCACCCCAAGGAGCATTTATGGGGTCGGATGACGCCTACAC-GTACTTTGTGAAGGGCTCCCGCTATTGGCAGTTCGACAACCGC-CAGCTGCGCGTCACCCCGGGTTACCCCAAATCCCTGCTCCGCG-AT-3′, which corresponds to the region of the coding sequence from 901-1453 (Yang et al., 2008). This sequence was amplified using forward primer 5′-GACGGCGGCTTCGATACCA-3′ and a reverse primer 5′-A-TCGCGGAGCAGGGATTT-3′, and cloned in pGEM vector. Sox10 probe (Cheng et al., 2000)

Neural crest culture

The 10-somite posterior regions of chicken embryos were dissected using a scalpel and placed in Dispase II (StemCell, 07923) at 1 U/ml for 30-40 min. Neural tube explants were dissected using tungsten needles and cultured in an IBIDI eight-well chamber µ-slide (IBIDI 80821) coated with fibronectin (Sigma F1141, 10 µg/ml). Wells were filled with DMEM (Gibco 61962-026)/10% newborn calf serum/penicillin-streptomycin (Thermofisher 15140122) at 10 units with sirDNA (SpiroChrome SC007, 1/500). Neural tube explants were incubated at 38°C with 5% CO_2 overnight. For MMP14 inhibition, neural tube explants were incubated for 16 h with DMSO or NSC405020 (Millipore 444295) at 0.5 mM.

Western blot

The protein samples were prepared from chick embryo electroporated at stage HH12 and harvested 24 h later. Control embryos were at the equivalent stage. Neural tubes were dissected with dispase (StemCell, 07923) at 1 U/ml 30-45 min at 37°C. Neural tubes were lysed with lysis buffer [10 mM Tris-Cl (pH 7.5), 150 mM NaCl, 0.5 mM EDTA, 0.1% SDS and anti-protease cocktail]. Protein samples were loaded in acrylamide gel (BioRad Mini-Protean TGX 4-15% 456-8084). Protein migration and transfer were carried out using Mini-PROTEAN Tetra Vertical Electrophoresis Cell for Mini Precast Gels, 4-gel (1658004), PowerPac HC High-Current Power Supply (1645052). Western blot antibodies used were: custom-made polyclonal mouse anti-chick MMP14 (1/2500), rabbit anti-tubulin (Cell Signaling, 2148, 1/1000), anti-mouse PAR3 and anti-human Par3 (Millipore 07-330 and 8E8, respectively, 1/1000; clone 8E8 did not recognize chick-Par3, 07-330 produced multiple non-specific bands on top of the expected 180, 150 and 100 kDa bands, rendering the blots inconclusive), mouse anti-GFP (Roche, 11814460001, 1/1000) and rabbit anti-GFP (Merck, G1544, 1/1000). Secondary antibodies used were: donkey anti-mouse HRP (Jackson ImmunoResearch, 715-035-150), donkey anti-rabbit HRP (Jackson ImmunoResearch, 711-035-152), used at 1/10,000.

FRET analysis

Chick MMP14 FRET probe was made by replacing human pro-MMP2 MMP14 cleavage site with a chicken pro-MMP2 MMP14 cleavage site in the human MMP14 FRET reporter (Ouyang et al., 2008). FRET acceptor photobleaching was performed on cryosections using a Zeiss 710 confocal microscope. Individual migratory NC cells located in ventromedial pathway were imaged at 514 and 454 nm, with a 40× objective at zoom 8 to acquire fluorescence from YPet and CFP, respectively. The CFP image was acquired at 70% of the dynamic range. The bleaching module was then used to deliver a series of fast illuminations at 514 nm at 100% to bleach YPet. Bleaching automatically stops when the YPet intensity reaches 20% of its initial intensity (typically 5 to 10 illuminations, total bleaching time of ∼2-5 s). Then, YPet and CFP are imaged again with the same settings as the pre-bleach images. FRET index is calculated using FIJI/ImageJ. Each image was converted to 32-bit and thresholded, and the background was set to NaN. Mean gray level intensity are calculated on the whole image for CFP pre-bleaching and post-bleaching images. Then the following calculation was carried out in Excel [(CFPpost-CFPpre)/CFPpost]×100=FRET index.

Chick MMP14 expression vectors

Full-length MMP14 was synthetized by GenScript using codon optimization to reduce the amount of GCs. Deletions of the catalytic domain, the cytoplasmic tail and the point mutant forms were made by PCR strategies from the optimized sequence and subcloned into the pCAGGS vector for electroporation.

Image acquisition and analysis

Images were captured using a stereomicroscope Leica MZF10F equipped with a Leica DFC450C camera and LAS software, a Nikon Eclipse 80i equipped with a DXM1200C camera and the NIS-elements software, a Zeiss AxioImager 2 equipped with a Hamamatsu ORCA Flash 4 camera and the Zen2 software, and a confocal Zeiss 710. Images were then processed using FIJI.

Analysis of cell migration

On cryosections, we measured the net dorsoventral distance of the most dorsal GFP^+ cell (d) and the dorsoventral length of neural tube (D) on the corresponding section. We calculated the net distance of the most dorsal GFP^+ cells with the ratio r=d/D (Fig. S11). On NC cultures, we analyzed cell dispersion by dividing the area explored by the GFP^+ cell area by that explored by $SiR\text{-}DNA^+$ cells. To measure the area, a line was drawn to link all outer GFP^+ cells together. The same was done for $siR\text{-}DNA^+$ cells (Fig. S12).

Statistics

Statistical analyses were performed using Prism 6 (GraphPad). Datasets were tested for Gaussian distribution. Student's *t*-tests or ANOVA followed by multiple comparisons were used with the appropriate parameters depending on the Gaussian versus non-Gaussian characteristics of the data distribution. Significance threshold was set at $P<0.05$. Proportions were compared according to Taillard et al. (2008). For the box and whisker plots, the box extends from the 25th to the 75th percentile, and the whiskers show the extent of the whole dataset. The median is plotted as a line inside the box.

Acknowledgements

We thank Dr Andreas Merdes (CNRS UMR5547, Toulouse) for the kind gift of PCM1 antibody. We are grateful to Dr Hervé Acloque for advice and for critical reading of the manuscript. We thank Dr Daniela Roellig for reagents and critical reading of the manuscript, and Dr Céline Cougoule for friendly advice throughout the project.

Competing interests

The authors declare no competing or financial interests.

Author contributions

Conceptualization: C.A., E.T.; Methodology: C.A., A.M., E.T.; Validation: C.A.; Formal analysis: C.A., E.T.; Investigation: C.A., A.M., A.B., E.D.-G., D.A., E.T.; Resources: D.A.; Data curation: C.A., A.M., E.T.; Writing - original draft: C.A., D.A., E.T.; Writing - review & editing: C.A., A.M., E.T.; Supervision: E.T.; Project administration: E.T.; Funding acquisition: D.A., E.T.

Funding

This work was supported by grants from the Fondation pour la Recherche Médicale (FRM AJE201224), the Conseil Régional Midi-Pyrénées (13053025), the Toulouse Cancer Santé (DynaMeca), the Centre National de la Recherche Scientifique (CNRS) and the Université Paul Sabatier (to E.T.); and by National Institutes of Health grants (RO1DE016289 and R24OD021485 to D.A.). E.T. and A.B. are CNRS permanent staff members. E.D.-G. was a master's student supported by DynaMeca.

C.A. was the recipient of a PhD fellowship from the Ministère de l'Enseignement supérieur, de la Recherche et de l'Innovation, a PhD Fellowship extension from the Association pour la Recherche sur le Cancer (ARC) and an international exchange grant from the Université Toulouse III - Paul Sabatier (ATUPS). Deposited in PMC for release after 12 months.

Supplementary information

Supplementary information available online at
http://dev.biologists.org/lookup/doi/10.1242/dev.183954.supplemental

References

Afonso, C. and Henrique, D. (2006). PAR3 acts as a molecular organizer to define the apical domain of chick neuroepithelial cells. *J. Cell Sci.* **119**, 4293-4304. doi:10.1242/jcs.03170

Ahlstrom, J. D. and Erickson, C. A. (2009). The neural crest epithelial-mesenchymal transition in 4D: a 'tail' of multiple non-obligatory cellular mechanisms. *Development* **136**, 1801-1812. doi:10.1242/dev.034785

Barbolina, M. V. and Stack, M. S. (2008). Membrane type 1-matrix metalloproteinase: substrate diversity in pericellular proteolysis. *Semin. Cell Dev. Biol.* **19**, 24-33. doi:10.1016/j.semcdb.2007.06.008

Barriga, E. H., Maxwell, P. H., Reyes, A. E. and Mayor, R. (2013). The hypoxia factor Hif-1alpha controls neural crest chemotaxis and epithelial to mesenchymal transition. *J. Cell Biol.* **201**, 759-776. doi:10.1083/jcb.201212100

Bonnans, C., Chou, J. and Werb, Z. (2014). Remodelling the extracellular matrix in development and disease. *Nat. Rev. Mol. Cell Biol.* **15**, 786-801. doi:10.1038/nrm3904

Burstyn-Cohen, T. and Kalcheim, C. (2002). Association between the cell cycle and neural crest delamination through specific regulation of G1/S transition. *Dev. Cell* **3**, 383-395. doi:10.1016/S1534-5807(02)00221-6

Cao, J., Chiarelli, C., Richman, O., Zarrabi, K., Kozarekar, P. and Zucker, S. (2008). Membrane type 1 matrix metalloproteinase induces epithelial-to-mesenchymal transition in prostate cancer. *J. Biol. Chem.* **283**, 6232-6240. doi:10.1074/jbc.M705759200

Castro-Castro, A., Marchesin, V., Monteiro, P., Lodillinsky, C., Rossé, C. and Chavrier, P. (2016). Cellular and molecular mechanisms of MT1-MMP-dependent cancer cell invasion. *Annu. Rev. Cell Dev. Biol.* **32**, 555-576. doi:10.1146/annurev-cellbio-111315-125227

Caswell, P. T. and Zech, T. (2018). Actin-based cell protrusion in a 3D matrix. *Trends Cell Biol.* **28**, 823-834. doi:10.1016/j.tcb.2018.06.003

Chan, K. M., Wong, H. L. X., Jin, G., Liu, B., Cao, R., Cao, Y., Lehti, K., Tryggvason, K. and Zhou, Z. (2012). MT1-MMP inactivates ADAM9 to regulate FGFR2 signaling and calvarial osteogenesis. *Dev. Cell* **22**, 1176-1190. doi:10.1016/j.devcel.2012.04.014

Cheng, Y.-C., Cheung, M., Abu-Elmagd, M. M., Orme, A. and Scotting, P. J. (2000). Chick sox10, a transcription factor expressed in both early neural crest cells and central nervous system. *Brain Res. Dev. Brain Res.* **121**, 233-241. doi:10.1016/S0165-3806(00)00049-3

Chuykin, I., Ossipova, O. and Sokol, S. Y. (2018). Par3 interacts with Prickle3 to generate apical PCP complexes in the vertebrate neural plate. *eLife* **7**, e37881. doi:10.7554/eLife.37881

Cui, G., Cai, F., Ding, Z. and Gao, L. (2019). MMP14 predicts a poor prognosis in patients with colorectal cancer. *Hum. Pathol.* **83**, 36-42. doi:10.1016/j.humpath.2018.03.030

Dady, A. and Duband, J.-L. (2017). Cadherin interplay during neural crest segregation from the non-neural ectoderm and neural tube in the early chick embryo. *Dev. Dyn.* **246**, 550-565. doi:10.1002/dvdy.24517

Dady, A., Blavet, C. and Duband, J.-L. (2012). Timing and kinetics of E- to N-cadherin switch during neurulation in the avian embryo. *Dev. Dyn.* **241**, 1333-1349. doi:10.1002/dvdy.23813

Dammermann, A. and Merdes, A. (2002). Assembly of centrosomal proteins and microtubule organization depends on PCM-1. *J. Cell Biol.* **159**, 255-266. doi:10.1083/jcb.200204023

Dong, Y., Chen, G., Gao, M. and Tian, X. (2015). Increased expression of MMP14 correlates with the poor prognosis of Chinese patients with gastric cancer. *Gene* **563**, 29-34. doi:10.1016/j.gene.2015.03.003

Duong, T. D. and Erickson, C. A. (2004). MMP-2 plays an essential role in producing epithelial-mesenchymal transformations in the avian embryo. *Dev. Dyn.* **229**, 42-53. doi:10.1002/dvdy.10465

Farina, F., Gaillard, J., Guérin, C., Couté, Y., Sillibourne, J., Blanchoin, L. and Théry, M. (2016). The centrosome is an actin-organizing centre. *Nat. Cell Biol.* **18**, 65-75. doi:10.1038/ncb3285

Feinberg, T. Y., Rowe, R. G., Saunders, T. L. and Weiss, S. J. (2016). Functional roles of MMP14 and MMP15 in early postnatal mammary gland development. *Development* **143**, 3956-3968. doi:10.1242/dev.136259

Gálvez, B. G., Matías-Román, S., Yáñez-Mó, M., Sánchez-Madrid, F. and Arroyo, A. G. (2002). ECM regulates MT1-MMP localization with beta1 or alphavbeta3 integrins at distinct cell compartments modulating its internalization and activity on human endothelial cells. *J. Cell Biol.* **159**, 509-521. doi:10.1083/jcb.200205026

Garmon, T., Wittling, M. and Nie, S. (2018). MMP14 regulates cranial neural crest epithelial-to-mesenchymal transition and migration. *Dev. Dyn.* **247**, 1083-1092. doi:10.1002/dvdy.24661

Giovannone, D., Ortega, B., Reyes, M., El-Ghali, N., Rabadi, M., Sao, S. and de Bellard, M. E. (2015). Chicken trunk neural crest migration visualized with HNK1. *Acta Histochem.* **117**, 255-266. doi:10.1016/j.acthis.2015.03.002

Gonzalo, P., Guadamillas, M. C., Hernández-Riquer, M. V., Pollán, A., Grande-García, A., Bartolomé, R. A., Vasanji, A., Ambrogio, C., Chiarle, R., Teixidó, J. et al. (2010a). MT1-MMP is required for myeloid cell fusion via regulation of Rac1 signaling. *Dev. Cell* **18**, 77-89. doi:10.1016/j.devcel.2009.11.012

Gonzalo, P., Moreno, V., Gálvez, B. G. and Arroyo, A. G. (2010b). MT1-MMP and integrins: hand-to-hand in cell communication. *Biofactors* **36**, 248-254. doi:10.1002/biof.99

Gouignard, N., Andrieu, C. and Theveneau, E. (2018). Neural crest delamination and migration: looking forward to the next 150 years. *Genesis* **56**, e23107. doi:10.1002/dvg.23107

Gross, J. and Lapiere, C. M. (1962). Collagenolytic activity in amphibian tissues: a tissue culture assay. *Proc. Natl. Acad. Sci. USA* **48**, 1014-1022. doi:10.1073/pnas.48.6.1014

Hamburger, V. and Hamilton, H. L. (1992). A series of normal stages in the development of the chick embryo. 1951. *Dev. Dyn.* **195**, 231-272. doi:10.1002/aja.1001950404

Holmbeck, K., Bianco, P., Caterina, J., Yamada, S., Kromer, M., Kuznetsov, S. A., Mankani, M., Robey, P. G., Poole, A. R., Pidoux, I. et al. (1999). MT1-MMP-deficient mice develop dwarfism, osteopenia, arthritis, and connective tissue disease due to inadequate collagen turnover. *Cell* **99**, 81-92. doi:10.1016/S0092-8674(00)80064-1

Hoshino, D., Tomari, T., Nagano, M., Koshikawa, N. and Seiki, M. (2009). A novel protein associated with membrane-type 1 matrix metalloproteinase binds $p27^{kip1}$ and regulates RhoA activation, actin remodeling, and matrigel invasion. *J. Biol. Chem.* **284**, 27315-27326. doi:10.1074/jbc.M109.041400

Iyer, R. P., Patterson, N. L., Fields, G. B. and Lindsey, M. L. (2012). The history of matrix metalloproteinases: milestones, myths, and misperceptions. *Am. J. Physiol. Heart Circ. Physiol.* **303**, H919-H930. doi:10.1152/ajpheart.00577.2012

Jiang, A., Lehti, K., Wang, X., Weiss, S. J., Keski-Oja, J. and Pei, D. (2001). Regulation of membrane-type matrix metalloproteinase 1 activity by dynamin-mediated endocytosis. *Proc. Natl. Acad. Sci. USA* **98**, 13693-13698. doi:10.1073/pnas.241293698

Jobin, P. G., Butler, G. S. and Overall, C. M. (2017). New intracellular activities of matrix metalloproteinases shine in the moonlight. *Biochim. Biophys. Acta Mol. Cell Res.* **1864**, 2043-2055. doi:10.1016/j.bbamcr.2017.05.013

Joseph, J. P., Harishankar, M. K., Pillai, A. A. and Devi, A. (2018). Hypoxia induced EMT: a review on the mechanism of tumor progression and metastasis in OSCC. *Oral Oncol.* **80**, 23-32. doi:10.1016/j.oraloncology.2018.03.004

Kasemeier-Kulesa, J. C., McLennan, R., Romine, M. H., Kulesa, P. M. and Lefcort, F. (2010). CXCR4 controls ventral migration of sympathetic precursor cells. *J. Neurosci.* **30**, 13078-13088. doi:10.1523/JNEUROSCI.0892-10.2010

Khokha, R., Murthy, A. and Weiss, A. (2013). Metalloproteinases and their natural inhibitors in inflammation and immunity. *Nat. Rev. Immunol.* **13**, 649-665. doi:10.1038/nri3499

Kopinke, D., Roberson, E. C. and Reiter, J. F. (2017). Ciliary hedgehog signaling restricts injury-induced adipogenesis. *Cell* **170**, 340-351. doi:10.1016/j.cell.2017.06.035

Leonard, C. E. and Taneyhill, L. A. (2019). The road best traveled: neural crest migration upon the extracellular matrix. *Semin. Cell Dev. Biol.* **100**, 177-185. doi:10.1016/j.semcdb.2019.10.013

Mannello, F. and Medda, V. (2012). Nuclear localization of matrix metalloproteinases. *Prog. Histochem. Cytochem.* **47**, 27-58. doi:10.1016/j.proghi.2011.12.002

Mayor, R. and Theveneau, E. (2013). The neural crest. *Development* **140**, 2247-2251. doi:10.1242/dev.091751

McQuibban, G. A., Butler, G. S., Gong, J.-H., Bendall, L., Power, C., Clark-Lewis, I. and Overall, C. M. (2001). Matrix metalloproteinase activity inactivates the CXC chemokine stromal cell-derived factor-1. *J. Biol. Chem.* **276**, 43503-43508. doi:10.1074/jbc.M107736200

Moore, R., Theveneau, E., Pozzi, S., Alexandre, P., Richardson, J., Merks, A., Parsons, M., Kashef, J., Linker, C. and Mayor, R. (2013). Par3 controls neural crest migration by promoting microtubule catastrophe during contact inhibition of locomotion. *Development* **140**, 4763-4775. doi:10.1242/dev.098509

Nieto, M. A., Huang, R. Y.-J., Jackson, R. A. and Thiery, J. P. (2016). Emt: 2016. *Cell* **166**, 21-45. doi:10.1016/j.cell.2016.06.028

Nishimura, T. and Kaibuchi, K. (2007). Numb controls integrin endocytosis for directional cell migration with aPKC and PAR-3. *Dev. Cell* **13**, 15-28. doi:10.1016/j.devcel.2007.05.003

Ouyang, M., Lu, S., Li, X.-Y., Xu, J., Seong, J., Giepmans, B. N. G., Shyy, J. Y.-J., Weiss, S. J. and Wang, Y. (2008). Visualization of polarized membrane type 1 matrix metalloproteinase activity in live cells by fluorescence resonance energy transfer imaging. *J. Biol. Chem.* **283**, 17740-17748. doi:10.1074/jbc.M709872200

Pang, L., Li, Q., Li, S., He, J., Cao, W., Lan, J., Sun, B., Zou, H., Wang, C., Liu, R. et al. (2016). Membrane type 1-matrix metalloproteinase induces epithelial-to-

mesenchymal transition in esophageal squamous cell carcinoma: Observations from clinical and in vitro analyses. *Sci. Rep.* **6**, 22179. doi:10.1038/srep22179

Pegtel, D. M., Ellenbroek, S. I. J., Mertens, A. E. E., van der Kammen, R. A., de Rooij, J. and Collard, J. G. (2007). The Par-Tiam1 complex controls persistent migration by stabilizing microtubule-dependent front-rear polarity. *Curr. Biol.* **17**, 1623-1634. doi:10.1016/j.cub.2007.08.035

Pelletier, A. J., van der Laan, L. J. W., Hildbrand, P., Siani, M. A., Thompson, D. A., Dawson, P. E., Torbett, B. E. and Salomon, D. R. (2000). Presentation of chemokine SDF-1 alpha by fibronectin mediates directed migration of T cells. *Blood* **96**, 2682-2690. doi:10.1182/blood.V96.8.2682

Perris, R. and Perissinotto, D. (2000). Role of the extracellular matrix during neural crest cell migration. *Mech. Dev.* **95**, 3-21. doi:10.1016/S0925-4773(00)00365-8

Remacle, A. G., Golubkov, V. S., Shiryaev, S. A., Dahl, R., Stebbins, J. L., Chernov, A. V., Cheltsov, A. V., Pellecchia, M. and Strongin, A. Y. (2012). Novel MT1-MMP small-molecule inhibitors based on insights into hemopexin domain function in tumor growth. *Cancer Res.* **72**, 2339-2349. doi:10.1158/0008-5472.CAN-11-4149

Rodríguez, D., Morrison, C. J. and Overall, C. M. (2010). Matrix metalloproteinases: what do they not do? New substrates and biological roles identified by murine models and proteomics. *Biochim. Biophys. Acta* **1803**, 39-54. doi:10.1016/j.bbamcr.2009.09.015

Rozanov, D. V., Deryugina, E. I., Ratnikov, B. I., Monosov, E. Z., Marchenko, G. N., Quigley, J. P. and Strongin, A. Y. (2001). Mutation analysis of membrane type-1 matrix metalloproteinase (MT1-MMP). The role of the cytoplasmic tail Cys^{574}, the active site Glu^{240}, and furin cleavage motifs in oligomerization, processing, and self-proteolysis of MT1-MMP expressed in breast carcinoma cells. *J. Biol. Chem.* **276**, 25705-25714. doi:10.1074/jbc.m007921200

Saito, D., Takase, Y., Murai, H. and Takahashi, Y. (2012). The dorsal aorta initiates a molecular cascade that instructs sympatho-adrenal specification. *Science* **336**, 1578-1581. doi:10.1126/science.1222369

Sakamoto, T. and Seiki, M. (2010). A membrane protease regulates energy production in macrophages by activating hypoxia-inducible factor-1 via a non-proteolytic mechanism. *J. Biol. Chem.* **285**, 29951-29964. doi:10.1074/jbc.M110.132704

Sakamoto, T., Weng, J. S., Hara, T., Yoshino, S., Kozuka-Hata, H., Oyama, M. and Seiki, M. (2014). Hypoxia-inducible factor 1 regulation through cross talk between mTOR and MT1-MMP. *Mol. Cell. Biol.* **34**, 30-42. doi:10.1128/MCB.01169-13

Sato, H., Takino, T., Okada, Y., Cao, J., Shinagawa, A., Yamamoto, E. and Seiki, M. (1994). A matrix metalloproteinase expressed on the surface of invasive tumour cells. *Nature* **370**, 61-65. doi:10.1038/370061a0

Shi, F. and Sottile, J. (2011). MT1-MMP regulates the turnover and endocytosis of extracellular matrix fibronectin. *J. Cell Sci.* **124**, 4039-4050. doi:10.1242/jcs.087858

Shimizu-Hirota, R., Xiong, W., Baxter, B. T., Kunkel, S. L., Maillard, I., Chen, X.-W., Sabeh, F., Liu, R., Li, X.-Y. and Weiss, S. J. (2012). MT_1-MMP regulates the PI_3Kdelta.Mi-$_2$/NuRD-dependent control of macrophage immune function. *Genes Dev.* **26**, 395-413. doi:10.1101/gad.178749.111

Shoval, I., Ludwig, A. and Kalcheim, C. (2007). Antagonistic roles of full-length N-cadherin and its soluble BMP cleavage product in neural crest delamination. *Development* **134**, 491-501. doi:10.1242/dev.02742

Spear, P. C. and Erickson, C. A. (2012). Interkinetic nuclear migration: a mysterious process in search of a function. *Dev. Growth Differ.* **54**, 306-316. doi:10.1111/j.1440-169X.2012.01342.x

Suenaga, N., Mori, H., Itoh, Y. and Seiki, M. (2005). CD44 binding through the hemopexin-like domain is critical for its shedding by membrane-type 1 matrix metalloproteinase. *Oncogene* **24**, 859-868. doi:10.1038/sj.onc.1208258

Taillard, É. D., Waelti, P. and Zuber, J. (2008). Few statistical tests for proportions comparison. *Eur. J. Oper. Res.* **185**, 1336-1350. doi:10.1016/j.ejor.2006.03.070

Théveneau, E., Duband, J.-L. and Altabef, M. (2007). Ets-1 confers cranial features on neural crest delamination. *PLoS ONE* **2**, e1142. doi:10.1371/journal.pone.0001142

Turunen, S. P., Tatti-Bugaeva, O. and Lehti, K. (2017). Membrane-type matrix metalloproteases as diverse effectors of cancer progression. *Biochim. Biophys. Acta Mol. Cell Res.* **1864**, 1974-1988. doi:10.1016/j.bbamcr.2017.04.002

Uekita, T., Itoh, Y., Yana, I., Ohno, H. and Seiki, M. (2001). Cytoplasmic tail-dependent internalization of membrane-type 1 matrix metalloproteinase is important for its invasion-promoting activity. *J. Cell Biol.* **155**, 1345-1356. doi:10.1083/jcb.200108112

Yang, M., Zhang, B., Zhang, L. and Gibson, G. (2008). Contrasting expression of membrane metalloproteinases, MT1-MMP and MT3-MMP, suggests distinct functions in skeletal development. *Cell Tissue Res.* **333**, 81-90. doi:10.1007/s00441-008-0619-3

Yao, G., He, P., Chen, L., Hu, X., Gu, F. and Ye, C. (2013). MT1-MMP in breast cancer: induction of VEGF-C correlates with metastasis and poor prognosis. *Cancer Cell Int.* **13**, 98. doi:10.1186/1475-2867-13-98

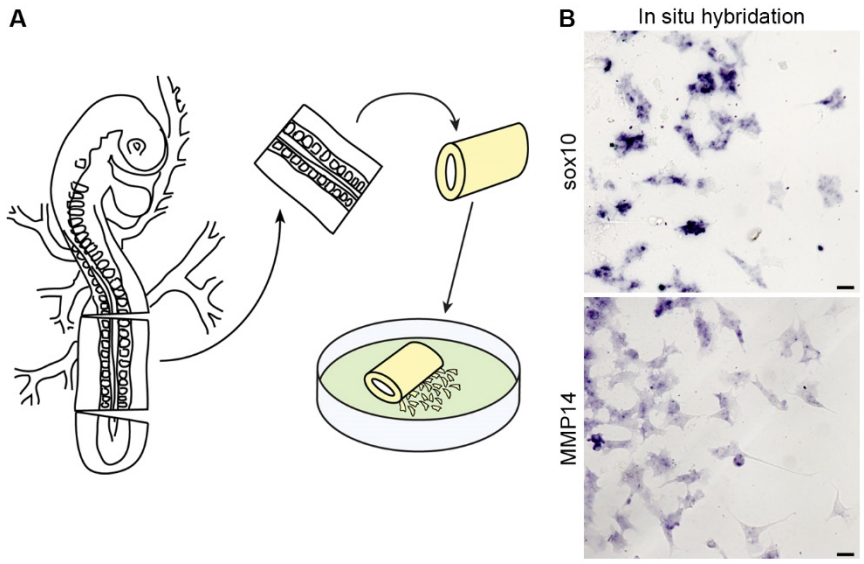

Figure S1: Expression of MMP14 in migratory neural crest cells

A, Diagram summarizing the neural crest explant procedure. B-C, culture of trunk neural crest cells on fibronectin. B, in situ hybridization for sox10 (upper panel) and chick MMP14 (bottom panel). Scale bars: 20 µm.

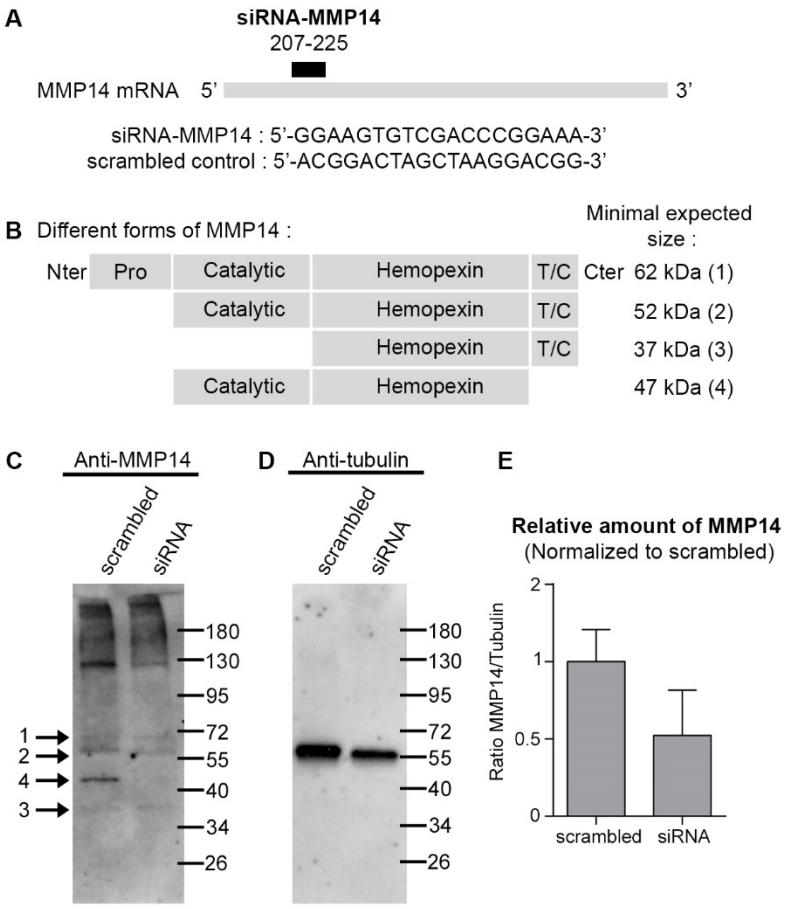

Figure S2: Validation of siRNA-MMP14 efficiency by western blot

A, diagram showing the position of the siRNA designed against chick MMP14. B, diagram depicting the expected minimal size of activated and processed MMP14. C, western blot for MMP14 from total neural tube extracts from embryos electroporated on one side with scrambled control or siRNA-MMP14 at stage HH12 and harvested 24 hours later. D, western blot for tubulin from the samples shown in C. E, relative amount of MMP14 to Tubulin in each condition normalized to scrambled control. Western blots were performed twice from independent protein samples. Note that since protein extracts were made from neural tubes electroporated unilaterally the expected maximum knockdown efficiency is 50%.

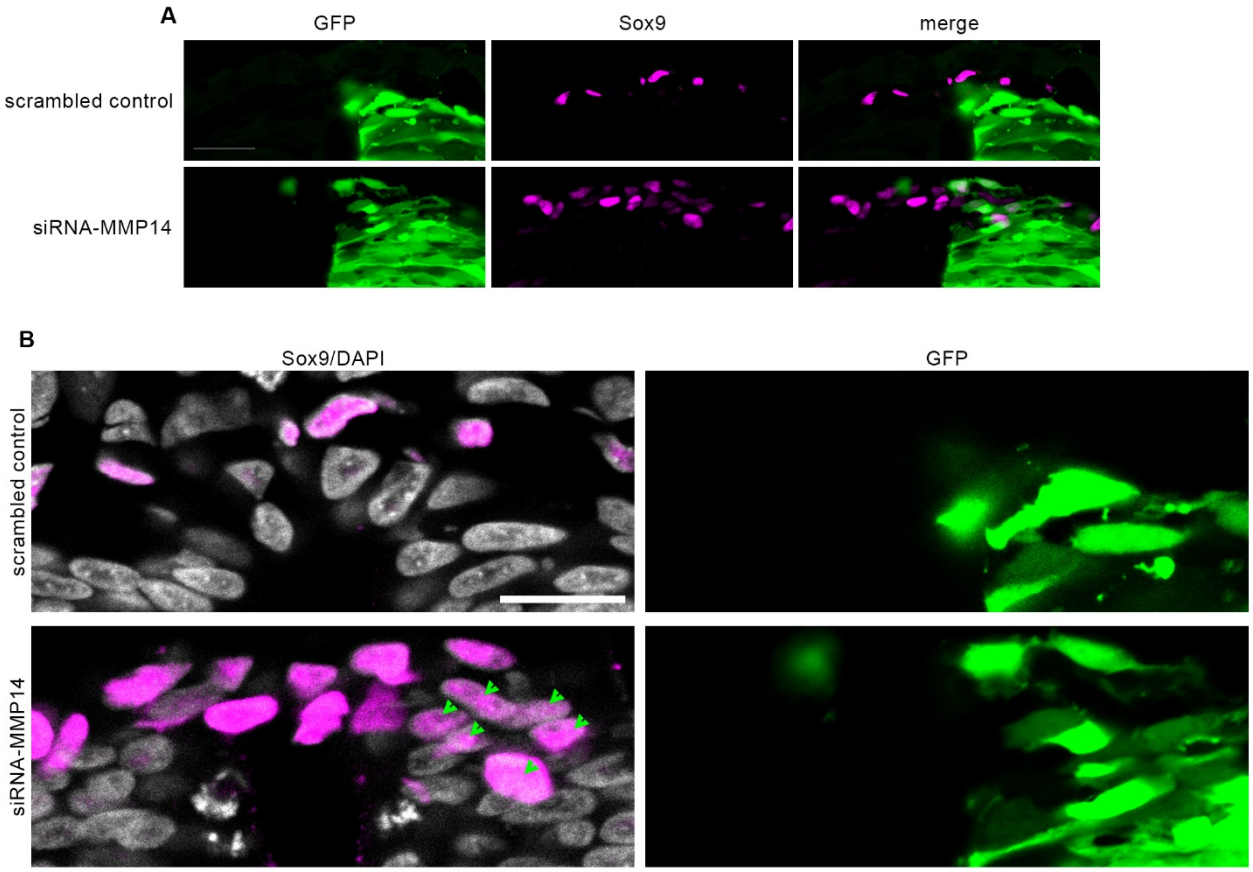

Figure S3: Knocking-down MMP14 leads to the accumulation of Sox9+ NC cells in the dorsal neural tube

A-B, immunostaining for Sox9 (magenta) after electroporation of the scrambled control or siRNA-MMP14. Electroporated side is visualized by GFP (green). B, zooms in the dorsal region of neural tube. Arrow heads indicate NC cells accumulated on the siRNA-MMP14 side. Scale bars: 50 µm in A, 20 µm in B.

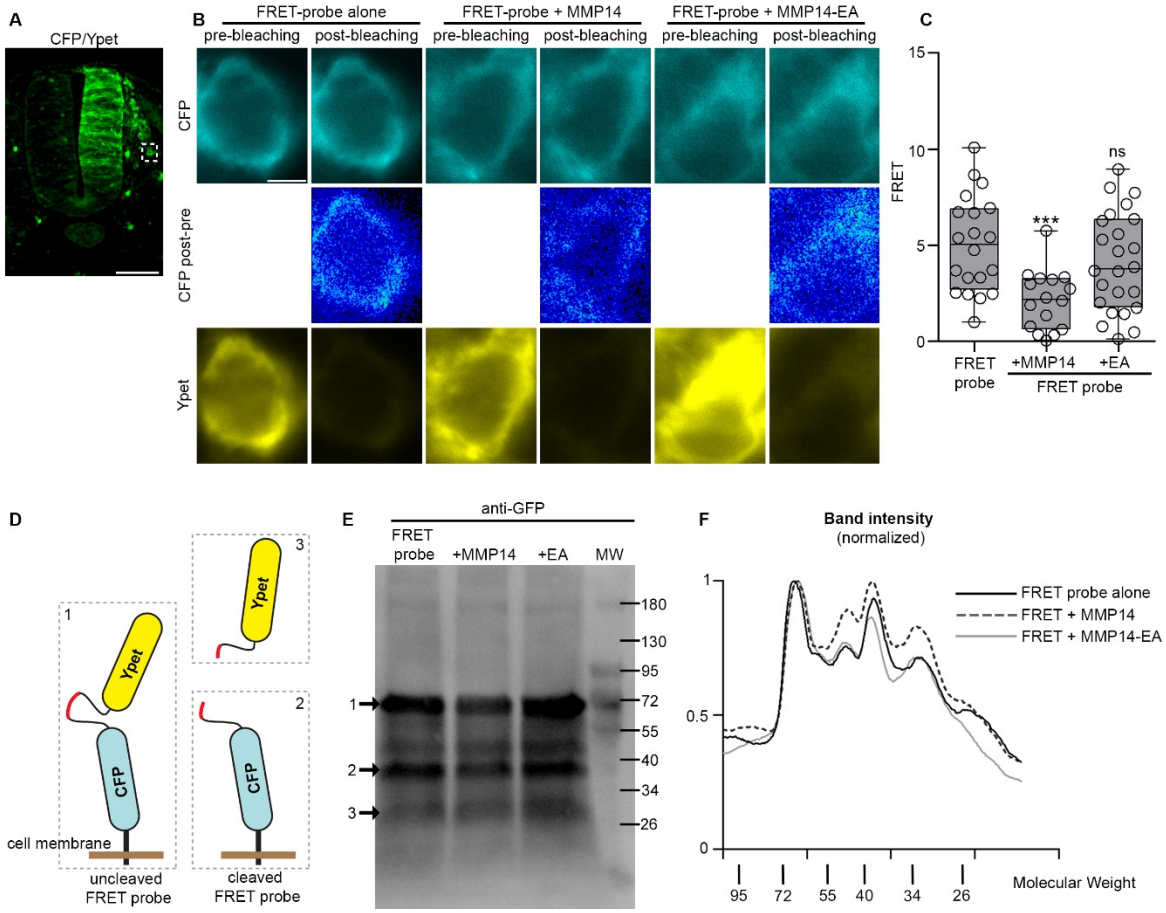

Figure S4: E-to-A point mutation in the catalytic domain of MMP14 abolishes its catalytic activity.

A, Confocal image of a transversal section of the neural tube 24h post-electroporation with the FRET reporter showing expression in the neural tube and in migratory NC cells (box), scale bar: 60 µm. B, representative pre- and post-bleaching confocal images of the CFP and YPet channels in single migratory NC cells expressing the FRET probe alone, the FRET probe + wild-type MMP14 or the FRET probe + MMP14-EA, scale bar: 2.5 µm. C, Graph of FRET efficiency for all three conditions. FRET probe alone (n_{cell}=20), FRET probe + MMP14 (n_{cell}=16) and FRET probe + MMP14-EA (n_{cell}=24) from one experiment. One-way Anova with multiple comparison *** (FRET probe alone vs FRET probe + MMP14) p=0.0005 and ns (FRET probe alone vs FRET probe + MMP14-EA) p=0.1921. C, diagram showing uncleaved FRET probe (1), cleaved FRET probe (2) and soluble Ypet (3). D, western blot using anti-GFP antibody to recognize all CFP- and YPet-containing fragments from total neural tube extracts from embryos electroporated with the FRET probe alone, the FRET probe and MMP14 or the FRET probe and MMP14-EA. Arrows indicate the different FRET forms shown in C. D, plot of normalized intensity of western blot bands with the FRET probe alone (black line), the FRET + MMP14 (dotted line) and the FRET + MMP14-EA (grey line). Data from one experiment (7 embryos per conditions). Note that expression of MMP14 leads to an increase of the intensity of the bands corresponding to the cleaved forms (2 and 3) compared to control and MMP14-EA expression.

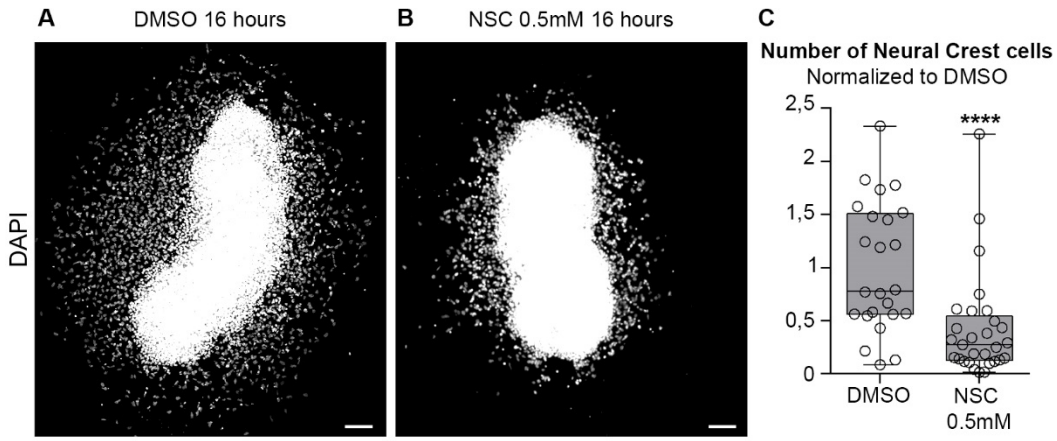

Figure S5: MMP14 inhibition affects delamination

A-B, Neural crest culture incubated 16 hours with DMSO (A) or MMP14 inhibitor NSC405020 at 0.5 mM (B) counterstained with DAPI. Scale bar: 100 µm. C, Graph of neural crest number with DMSO (24 explants) and NSC (29 explants) from five independent experiments. Unpaired Mann-Whitney test, ****p<0.0001.

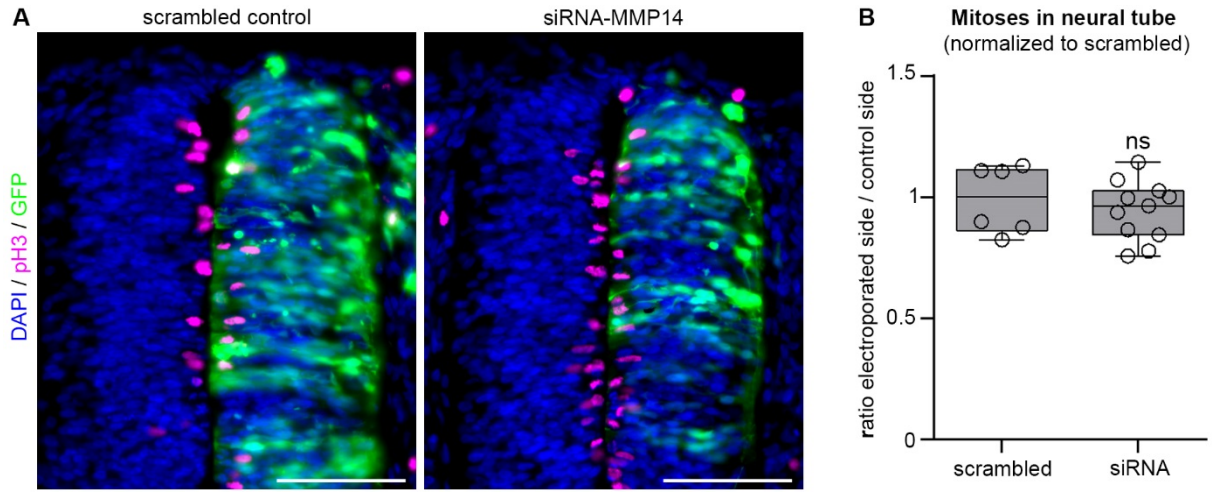

Figure S6: The loss of MMP14 does not increase cell proliferation.

A, immunostaining against phospho-histone 3 (pH3, magenta) after electroporation with scrambled control and siRNA-MMP14, counterstained with DAPI (blue). Electroporated side is visualized by GFP (green). Scale bar: 60 µm. B, Graph of mitoses in the neural tube with scrambled control ($n_{embryos}$= 6, $n_{sections}$= 112, $n_{mitoses}$= 1229 in control side and 1248 in electroporated side) and siRNA ($n_{embryos}$= 11, $n_{sections}$= 209, $n_{mitoses}$= 1773 in control side and 1676 in electroporated side) from four independent experiments. Unpaired T-test with Welch's correction ns p= 0.5096.

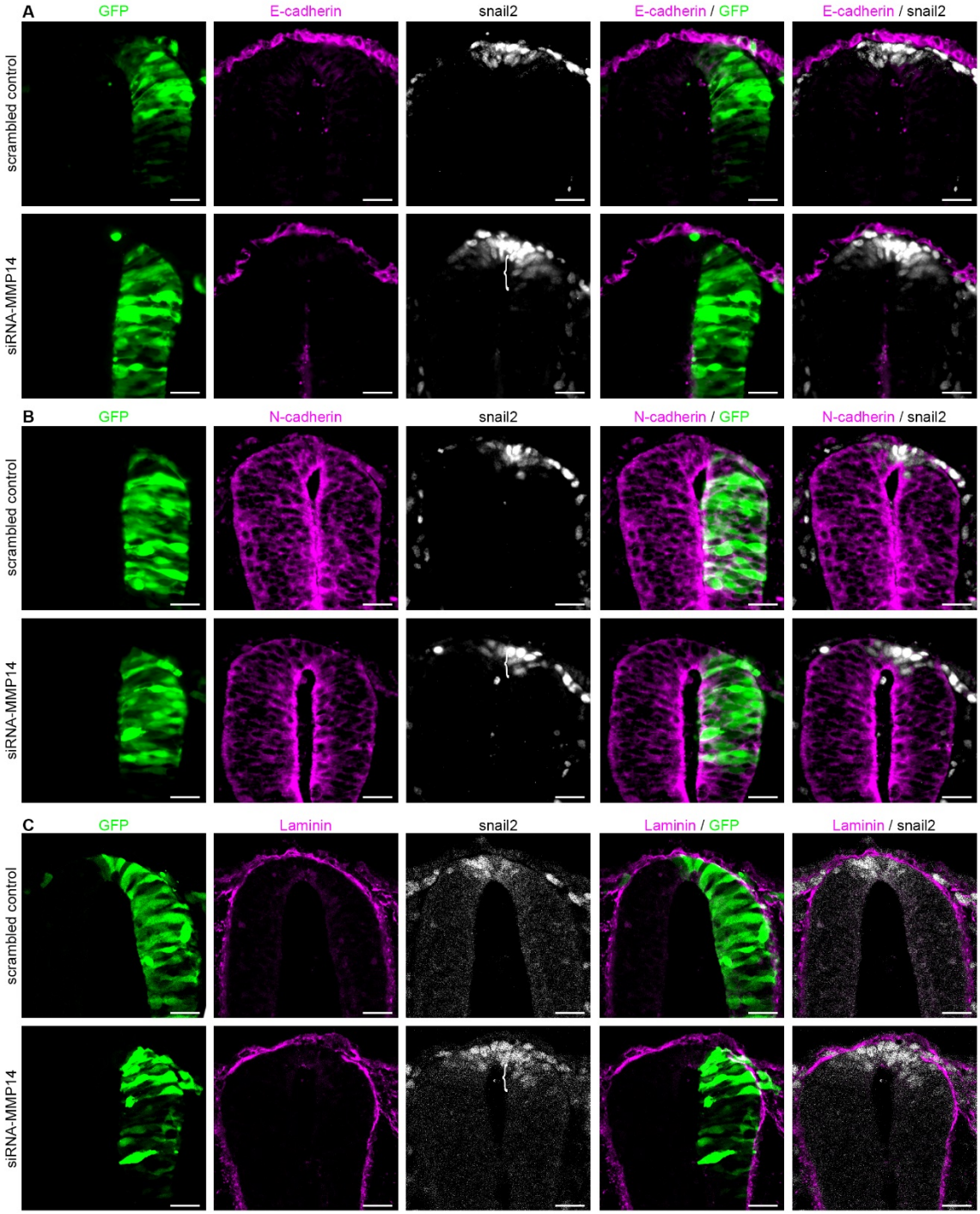

Figure S7: siRNA-MMP14 has no effects on E-Cadherin, N-Cadherin and laminin.

A-C, immunostaining against E-cadherin (magenta)(A) or N-cadherin (magenta)(B) or laminin (magenta)(C) and snail2 (grey) after electroporation with scrambled control (A-C, $n_{embryos}$= 5 from one experiment) and siRNA-MMP14 (A-C, $n_{embryos}$= 3 from one experiment). Electroporated side is visualized by GFP (green). The brackets indicate the accumulation of neural crest cells. Scale bars: 20 µm.

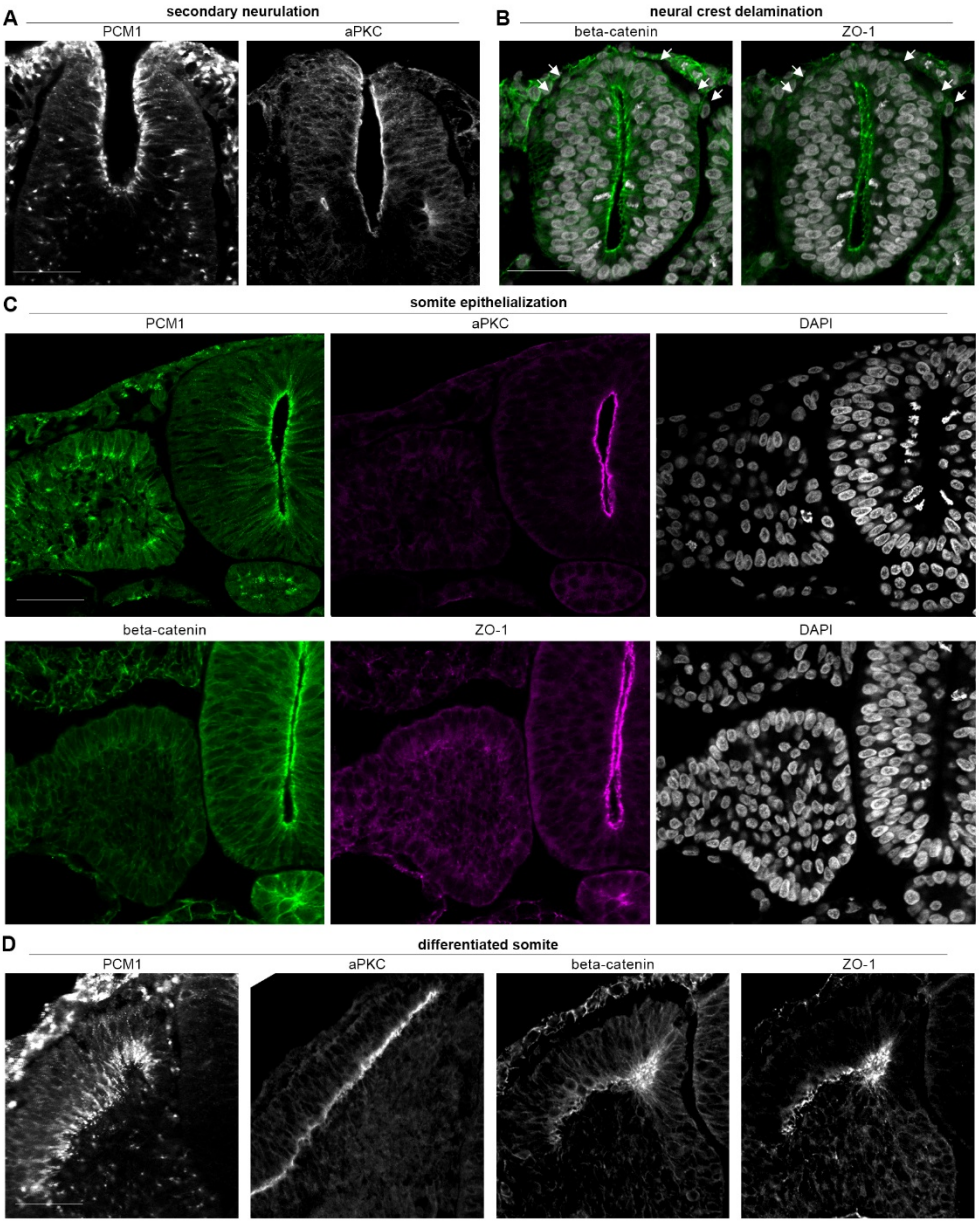

Figure S8: Validation of PCM1 as a marker to follow epithelial-mesenchymal plasticity during development.

A, Immunostainings against PCM1 and aPKC during secondary neurulation. B, Immunostainings for βcatenin and ZO-1 at the time neural crest delamination (arrowheads mark migrating NC cells along the neural tube). C, Immunostainings for PCM1, ZO-1, aPKC and βcatenin at the time of somite epithelialization. D, Immunostainings for PCM1, ZO-1, aPKC and βcatenin in differentiated somites. Note that PCM1 accumulates apically early on during epithelialization and remains detectable in mesenchymal cells whereas aPKC, ZO-1 and βcatenin only stain the apical poles of well-established epithelial structures. Scale bars: 40 µm in A, B and C; 30 µm in D.

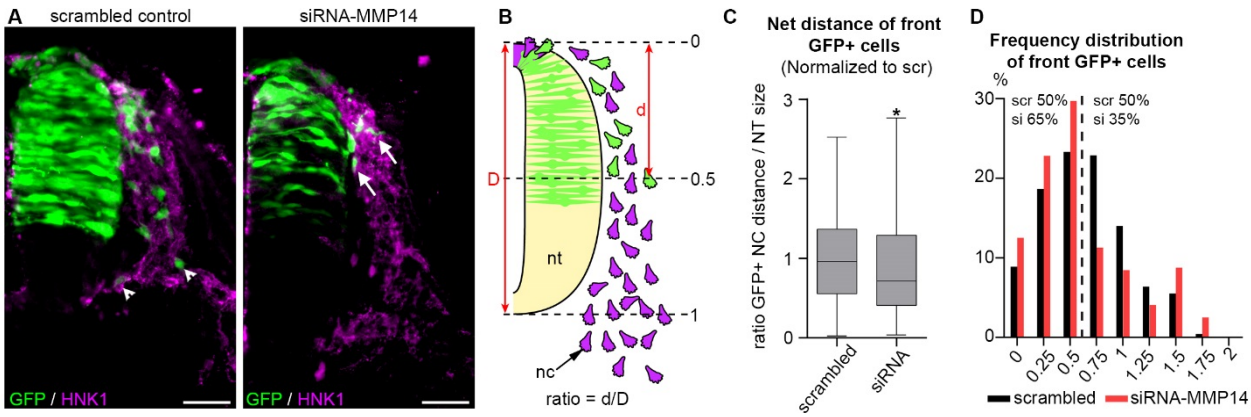

Figure S9: MMP14 is required for Neural Crest migration in vivo

A, immunostaining against HNK1 (magenta) on embryos electroporated with the scrambled control (left panel) or siRNA-MMP14 (right panel). Electroporated side is visualized by GFP (green). Arrowheads (scrambled) and arrow (siRNA-MMP14) indicate GFP+ neural crest cells at the front of neural crest streams. Scale bar: 40 µm. B, diagram depicting the method for measuring the distance migrated by GFP+ neural crest cells. The net dorsoventral distance of each GFP+ cells (d) was divided by the dorsoventral length of the neural tube on the corresponding transverse section, to correct for size differences across samples. A ratio of 0 means that neural crest cells were close to the dorsal part of the neural tube. A ratio of 1 indicates that NC cells were close to the ventral part of the neural tube. A ratio superior to 1, indicates that NC cells migrated beyond the ventral limit of the neural tube. C, ratio of front GFP+ neural crest cells distance over neural tube size. D, Frequency distribution of distances migrated by front GFP+ NC cells. Note that with the scrambled control 50% of the cells had a migration value between 0 and 0.5 whereas in siRNA-MMP14 this proportion jumps to 65%. Conversely, 50% of cells transfected with the scrambled control had a migration value above 0.5 whereas with siRNA-MMP14 only 35% of cells had migrated that far. Scrambled controls ($n_{embryos}$=5, $n_{GPF+\ cell}$=236) and siRNA-MMP14 ($n_{embryos}$=7, $n_{GFP+\ cell}$=320) from three independent experiments. Unpaired Mann-Whitney test, *p=0.0194.

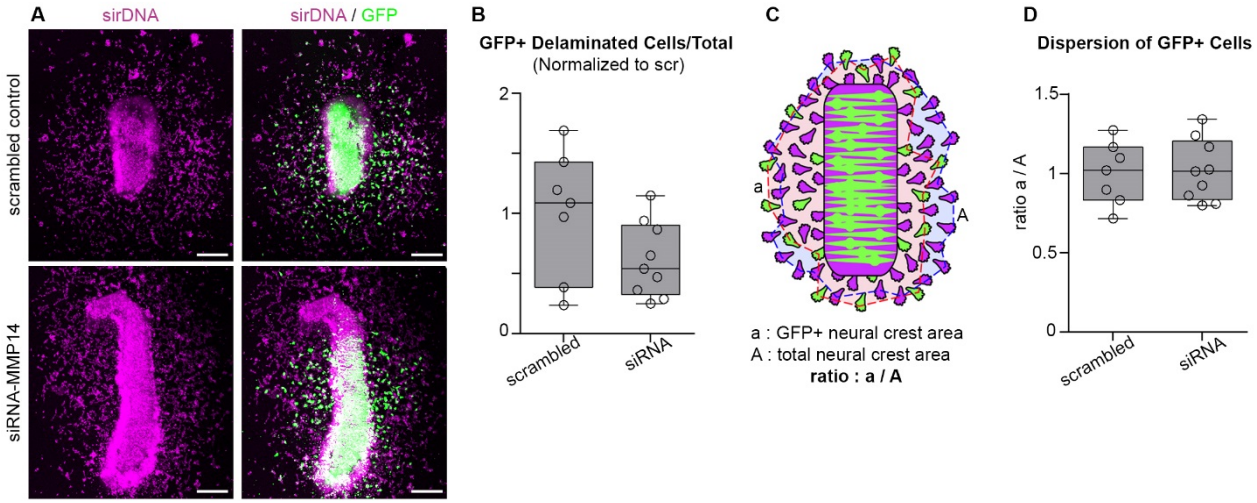

Figure S10: siRNA-MMP14 affects delamination but not motility

A, neural tube explants cultured on fibronectin coated dishes counterstained with sirDNA (magenta). Cells electroporated with the scrambled control (upper panels) or siRNA-MMP14 (bottom panels) are GFP-positive (green). Scale bar: 200 µm. B, ratio of GFP+ delaminated cells number over the total number of delaminated cells counted from sirDNA staining. Unpaired T-test with Welch's correction p=0.1186. C, Diagram explaining the method for measuring the dispersion of GFP+ cells. Area of GFP+ neural crest cells was divide by the area of all neural crest. D, ratio of GFP+ cells area over the total area from sirDNA staining. Unpaired T-test with Welch's correction p=0.8463. Scrambled control ($n_{explants}$=7) and siRNA-MMP14 ($n_{explants}$=9) from four independent experiments.

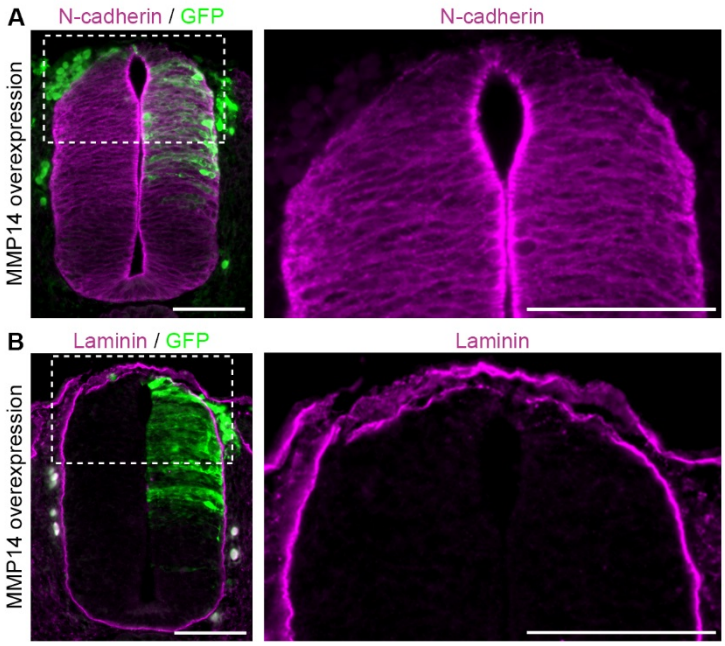

Figure S11: MMP14 overexpression is not sufficient to induce EMT-like phenotypes in the neuroepithelium.

A-B, Immunostaining against N-cadherin (A, magenta) and laminin (B, magenta) after overexpression of MMP14-GFP (green). Note that N-cadherin distribution is normal with a strong accumulation in the apical domain and that laminin is continuous along the basal domain. Dotted boxes indicate the position of the zoom. Representative images from 9 embryos analyzed from four independent experiments. Scale bar: 65 µm.

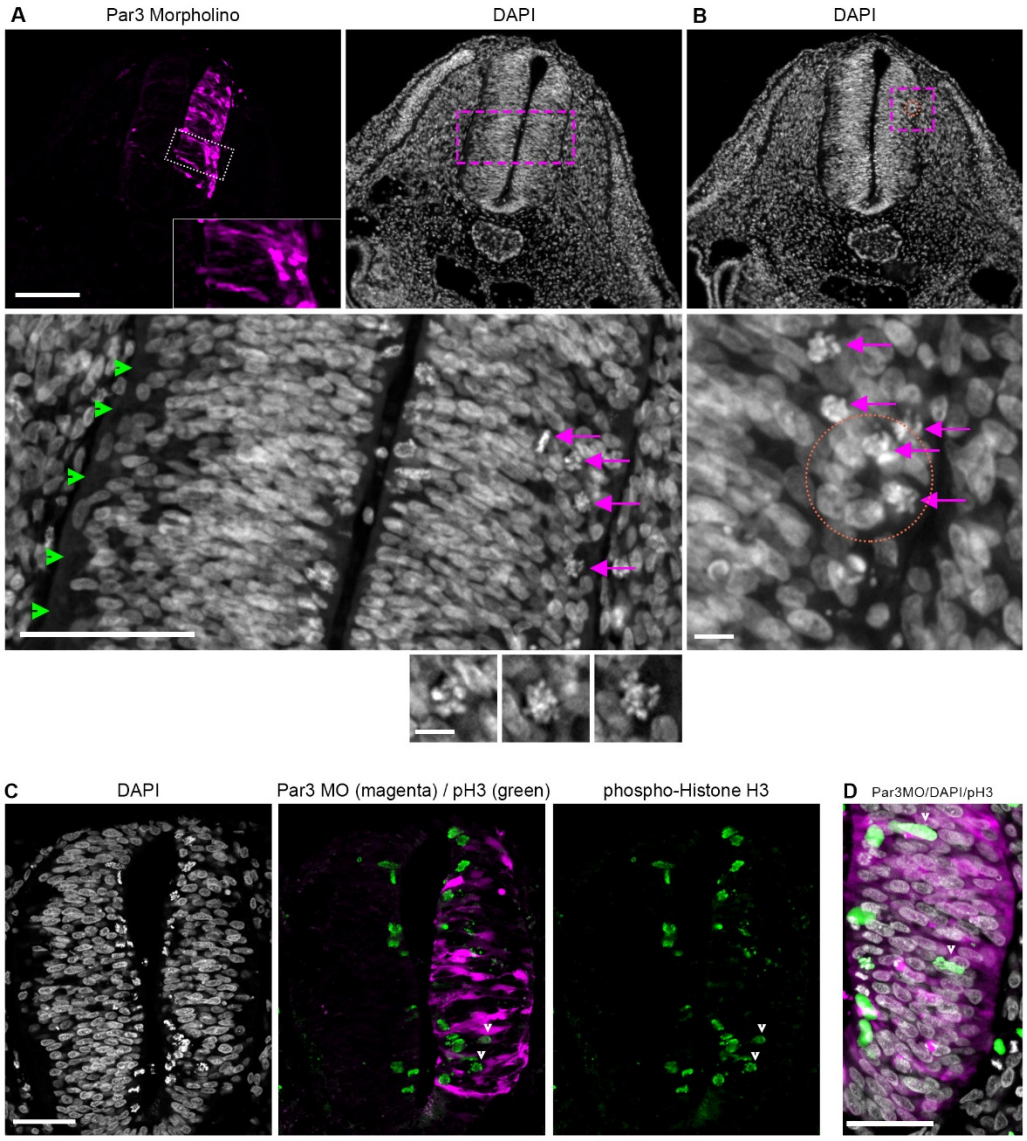

Figure S12. Electroporation of a translation-blocking Morpholino against chicken Par3 leads to polarity-related defects

A-B, transversal sections counterstained with DAPI (grey), Morpholino is in magenta showing basal accumulation of nuclei on the electroporated side compared to the control side. Note that the nuclei-free areas in the control side (green arrowheads) are no longer seen on the electroporated side. We also observed ectopic mitoses (magenta arrows and zooms underneath panel A). Note that MO-positive cells tend to accumulate basally (panel A and inset) and the occasional presence of rosette-like arrangements (brown dotted line in panel B) both suggesting some degree of apical detachment. C-D, pH3 immunostaining to detect mitoses (green), counterstain with DAPI (grey), Morpholino is in Magenta. Images on this figure come from 4 different embryos and summarize the observed defects in a batch of 7 embryos coming from two independent experiments.